~~SECRET~~

334

AGA LOG NO. 0404

COPY 8 OF 110 COPIES

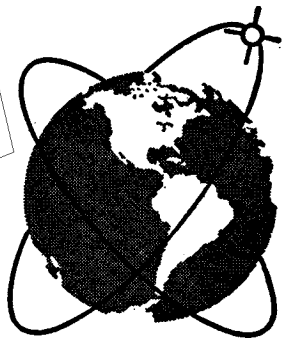

25X1

First Scientific Report

ITEM 11

Distributed Source Effects in LICOR System, Lightning Correlation Radar, Aero Geo Astro Corp.

DOC 01	REV DATE 18 JUL 1980	BY 018323	
ORIG COMP 201	OFI 56	TYPE 03	
ORIG CLASS S	PAGES 54	REV CLASS X	
JUST	NEXT REV	AUTH: HR 70-2	

~~Prepared for:~~

~~The Office of Naval Research~~

~~Under~~ Contract Nonr–3163(00)

5 August, 1960

TO 22 JAN 62

Aero Geo Astro
CORPORATION
ALEXANDRIA, VIRGINIA

[redacted]

~~SECRET~~

Declassified in Part - Sanitized Copy Approved for Release 2012/06/04 : CIA-RDP78-03172A000200010001-9

Errata Sheet, Scientific Report,
"Distributed Source Efforts in LICOR System"

Page No.	The material as it should read	
3	$R(T) \cos \omega T$	(1)
3	$\sin 2\pi/\lambda \ (u + a - b - d)$	(3)
5	$a + u - \lambda/2 < b + d < a + u$	(6)
5	$b + d = a + u - n\lambda/2 \quad n = 0 \pm 1 \pm 2 \ldots$	(7)
5	$b - a = (u - d) - n\lambda/2$	(8)
16	$Bn = \theta_n - \theta_{n-1} = \tan^{-1}\sqrt{\lambda/d}\ \sqrt{n} - \tan^{-1}\sqrt{\lambda/d}\ \sqrt{n-1}$ $= \tan^{-1} \dfrac{\sqrt{\lambda/d}\ (\sqrt{n} - \sqrt{n-1})}{1 + \lambda/d\ \sqrt{n(n-1)}}$	(18)
18	$Bn \doteq \sqrt{\lambda/d}\ (\sqrt{n} - \sqrt{n-1}\ )$	(19)
18	$Bn = \delta/(2p + 1) \quad p = 1, 2 \ldots$	(22)
18	$\tan \theta_N = \sqrt{\lambda/d\ N}$	(24)
20	$W = 2 \dfrac{r + d/2}{r} \sqrt{N\lambda d}$	(27)

AERO GEO ASTRO CORPORATION
Alexandria, Virginia

Scientific Report No. C60-1 22 July 1960

DISTRIBUTED SOURCE EFFECTS IN LICOR SYSTEMS

by

Donald J. Adrian

Prepared Under Office of Naval Research Contract 3163(00)

ABSTRACT

The effects of distributed sources in lightning correlation radars are discussed. It is shown that a large source results in a narrow region of maximum "target sensitivity"; while outside of this region, there are "minor lobes" of decreasing amplitude. The implications of the results, such as site selection and antenna directivity requirements, are discussed.

I. INTRODUCTION

Both VLF stations and lightning are used as sources of energy for missile trail and ionospheric perturbation detection. When distributed sources of atmospheric noise are used, the phase difference between the reference and reflected signals will not be the same for all lightning strokes. With a correlation radar, this results in a narrow region, or beam, as far as any reflected energy is concerned. These narrow regions occur for both back scatter and forward scatter. Outside of the main beam, there are other regions, or "minor lobes", of target sensitivity.

Source contours which will result in a constant phase difference at the radar are first derived. These are then used to obtain the "space patterns" of target sensitivity. The effects of these results on system operation and design are discussed.

II. DERIVATION OF CONSTANT PHASE REGIONS

The analysis presented in this section is an extension of work reported earlier by the author.[1]

We first consider an elementary lightning correlation system as shown in Figure 1. A wave from a source S is picked up on the reference antenna, amplified in a receiver, delayed an amount τ equivalent to a propagation distance u and fed to the correlator as a reference signal. The wave from S also travels a distance b to the missile M (Figure 2) and is reflected back a distance d to the radar R. This scattered signal is picked up on the antenna, amplified in the "scatter receiver" and then fed to the correlator. It can be shown that the signal out of the correlator (the system range gate) is of the form

$$R(\tau) \cos W\tau \tag{1}$$

where τ is the time difference between the two signals feeding the correlator. The exact form of $R(\tau)$ will depend somewhat on the receiver filter characteristics. In general, it will be similar to that shown in Figure 3. Equation (1) may be put in the form shown below by referring to Figure 2.

$$R\left[1/C\ (u + a - b - d)\right] \cos\ 2\pi/\lambda\ (u + a - b - d) \tag{2}$$

Our main interest here will be in the cosine term of equation (2). A lightning correlation system may also contain a quadrature channel in which the cosine term of equation (2) wouldbe replaced by

$$\sin 2\pi/\lambda\ (a + a - b - d) \tag{3}$$

---

1 D. J. Adrian, R. H. Espeland, H. H. Burroughs, Naval Ordnance Laboratory, Corona, "Mides Interim Report", TM-45-23.

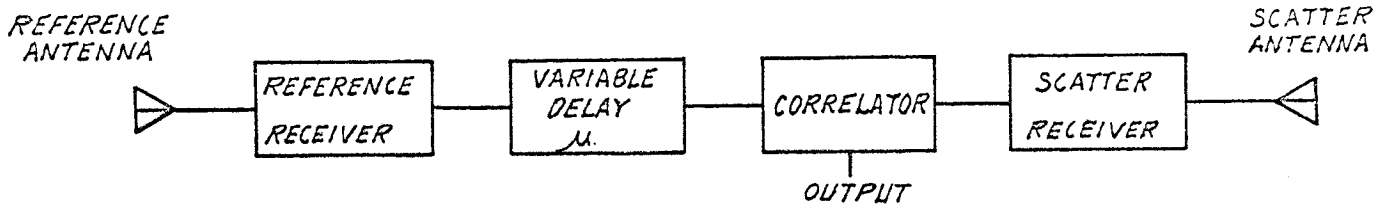

FIG. 1. ELEMENTARY SYSTEM

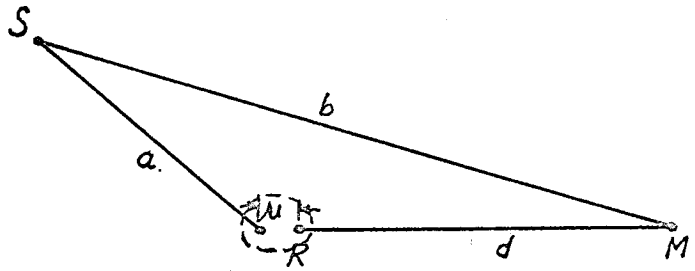

FIG. 2. SYSTEM GEOMETRY

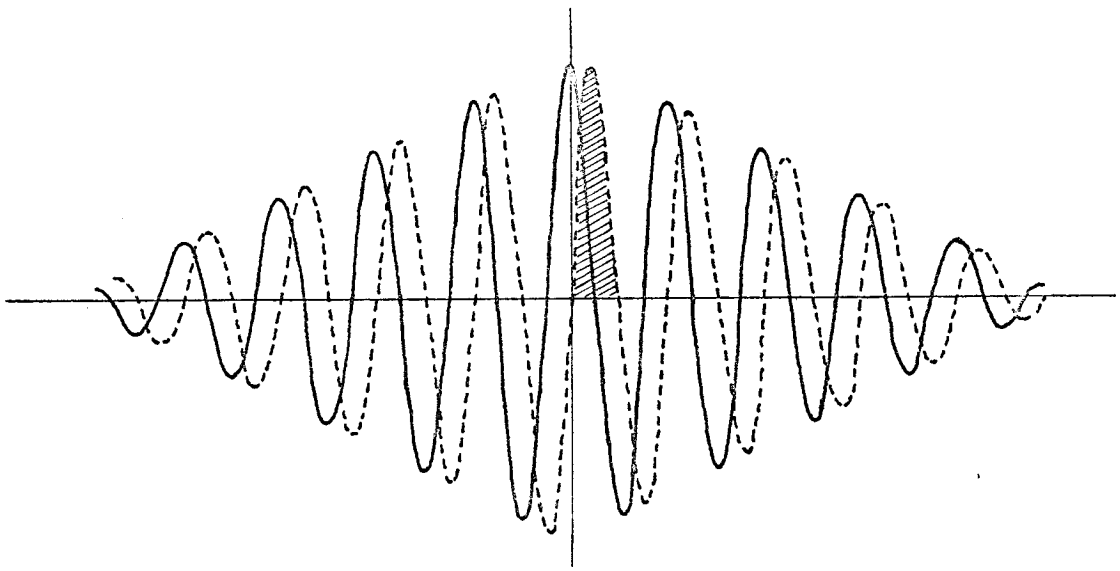

FIG. 3. RANGE GATE

Sources would contribute to the center lobe of equation (3) (shown crossed hatched in Figure 3) if they satisfy the following condition

$$a + u < b + d < a + u + \lambda/2 \tag{4}$$

The two adjacent negative lobes will result when

$$a + u + \lambda/2 < b + d < a + u + \lambda \tag{5}$$

or

$$a + w - \lambda/2 < b + d < a + w \tag{6}$$

the boundaries of the various regions are then given by

$$b + d = a + w - n\lambda/2 \qquad n + 0, \pm 1, \quad \pm 2 \tag{7}$$

or

$$b - a = (w - d) - n\lambda/2 \tag{8}$$

If we let the line d lie on the x axis, the family of hyperbolas described by equation (8) can be put in the standard form

$$x^2/A^2 - y^2/B^2 = 1 \tag{9}$$

where

$$A^2 = \frac{\left[u - d - n\lambda/2\right]^2}{4} \tag{10}$$

and

$$B^2 = 1/4 \left[n\lambda\,(u - d) - n\,(u - 2d) - (n\lambda/2)^2\right] \tag{11}$$

Examples of these hyperbolas are shown in Figure 4.

For sources located a large distance from the radar, the hyperbolas may be replaced by their asymptotes. The slope of the asymptotes is given by

$$\text{Slope} = \pm\, B/A = \sqrt{\frac{d^2 - (u - d - n\lambda/2)^2}{u - d - n\lambda/2}}$$

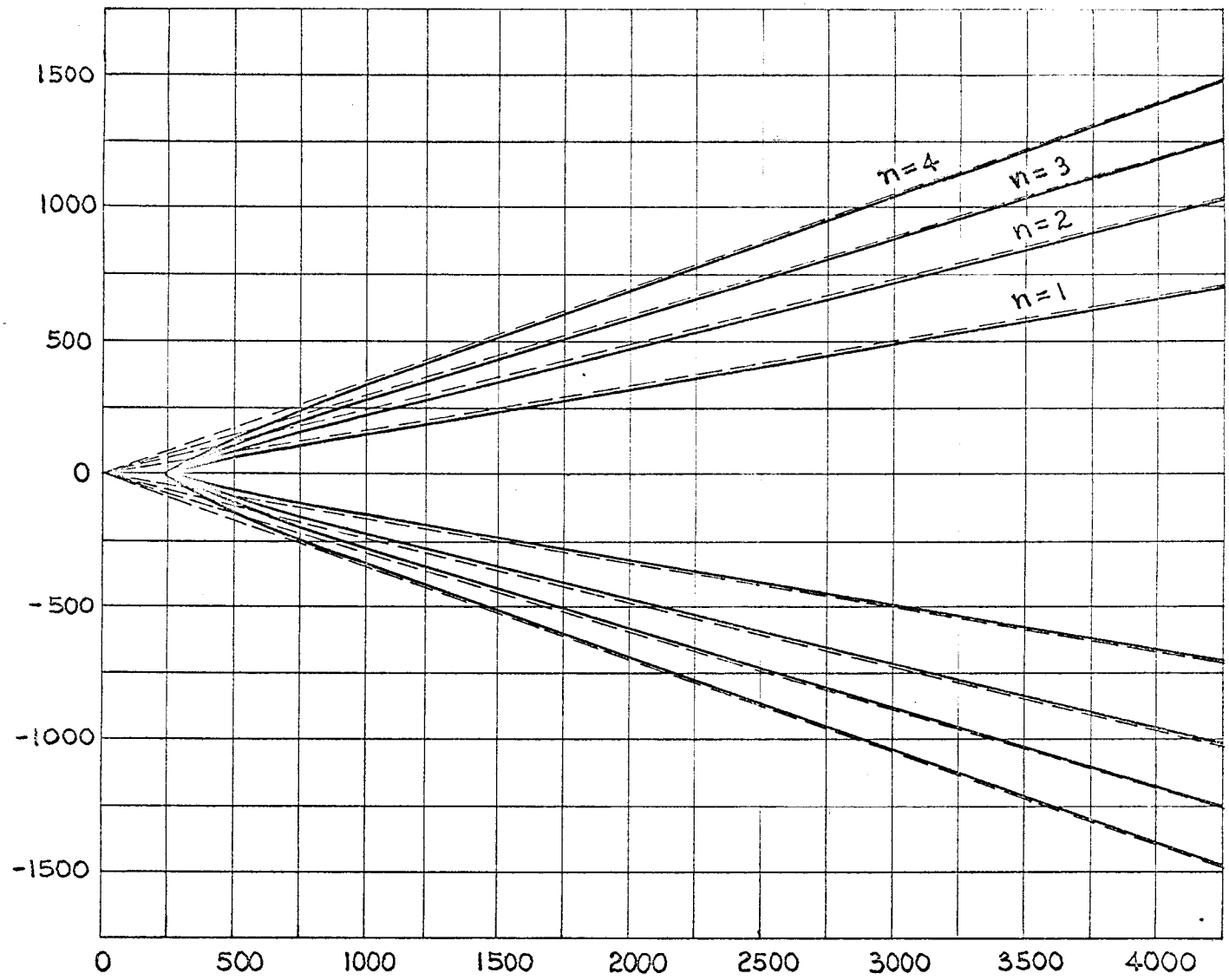

$$\sqrt{y^2+\left(x+\frac{d}{2}\right)^2} - \sqrt{y^2+\left(x-\frac{d}{2}\right)^2} = d - \frac{n\lambda}{2}$$

where $\lambda = 14$ and $d = 500$

FIG. 4.
CONSTANT PHASE DIFFERENCE CONTOURS

Next we let

$$u = 2d - m\lambda/2 \tag{13}$$

and obtain

$$\text{Slope} = \sqrt{\frac{d^2 - d - (m + n)\,\lambda/2}{d - (m + n)\,\lambda/2}} \tag{14}$$

If we let the internal time delay u be equivalent to 2d (m = 0 in equation (14)), then the regions contributing to the various lobes of the range function are obtained by letting "n" run through the integers. The graphs for various values of d are shown in Figures 5 through 12. Regions between the n = 1 lines contribute to the main lobe of the range function. Regions between n = 1 and n = 2 contribute to the first negative lobe. Regions between n = 2 and n = 3 contribute to the next positive lobe, etc. When the internal delay u is less than twice range ($u = 2d - m\,\lambda/2$), the main lobe of the range function will arise from sources between the m and m + 1 line, negative lobes between the m + 1 and the m + 2 lines and also between the m - 1 and m lines; thus the curves of Figures 5 through 12 are of universal use. It should also be noted that the simple radar indicates that the reflector is at a range

$$u/2 = d - m\lambda/4 \tag{15}$$

rather than at the true range d. Direction finding techniques could be used to correct for this small error.

III. DISTRIBUTED SOURCE EFFECTS

In this section we consider the distributed sources which occupy only a portion of the region between the two n = 1 lines. When the source is on n = 0 line, one of the correlator channels has zero output while the other one has a maximum output, as seen in Figure 3, thus all portions of the distributed source contribute approximately the same amount to the signal. As the source is revolved around the radar R, the magnitude of the signal out of the dual correlator would decrease. When the source just occupies the distance between two lines, it would contribute as a sinusoidal function with the center of the region giving a full contribution and the outer edges of the region giving zero contribution. The integral of a half period of a sine wave is $2/\pi$ so that a source in this location would contribute 0.637 of the amount of signal that it would if located on n = 0. As the source is revolved further, it arrives at a position where it just overlaps two regions. In this case, half of the source would yield a positive output while the other half would yield a negative output, thus yielding zero net output. When the source overlaps three regions, one-third of the total energy would contribute to the target signal; overlap of four regions would again yield zero output while overlap of five regions would yield one-fifth of the maximum output, etc.

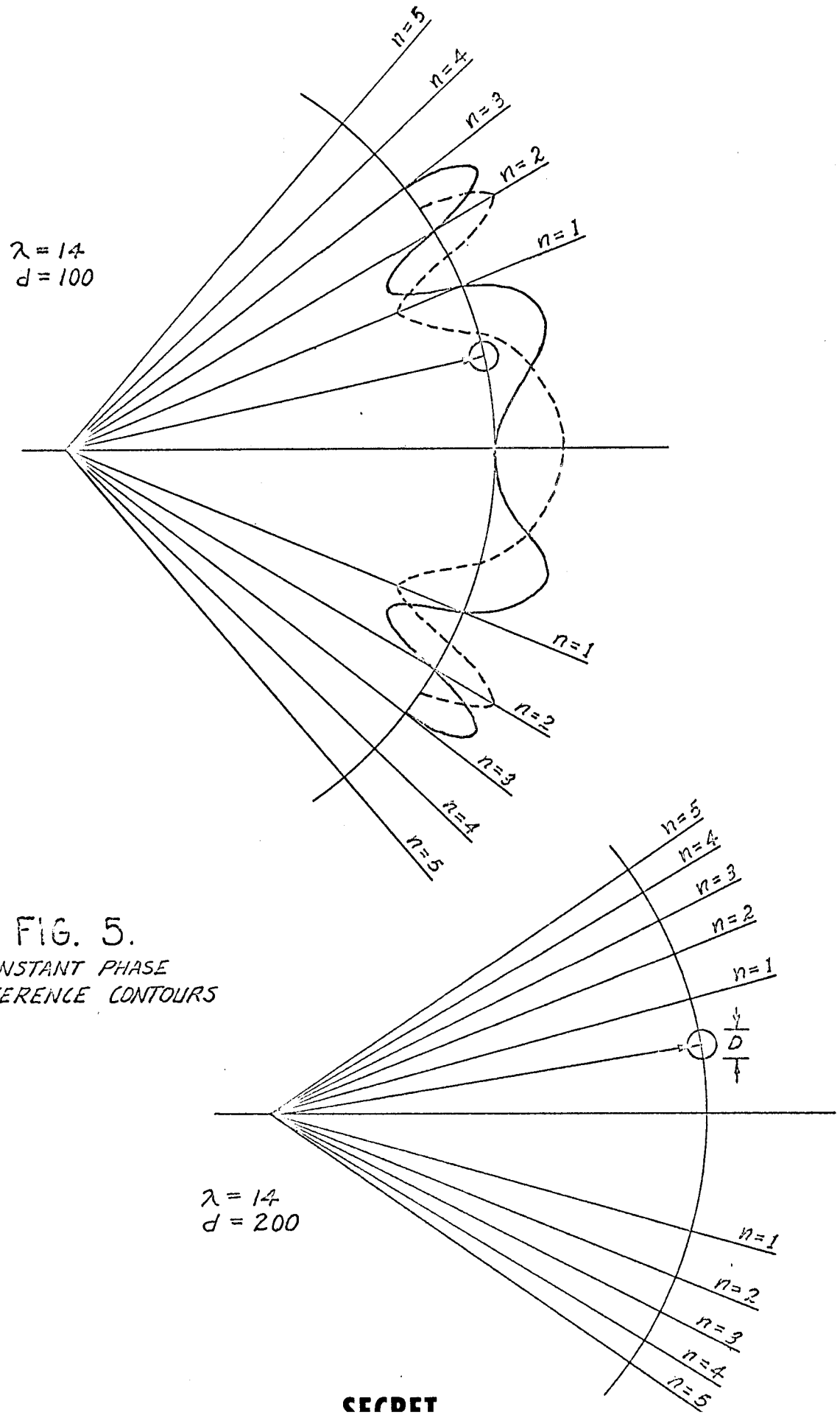

FIG. 5.
CONSTANT PHASE
DIFFERENCE CONTOURS

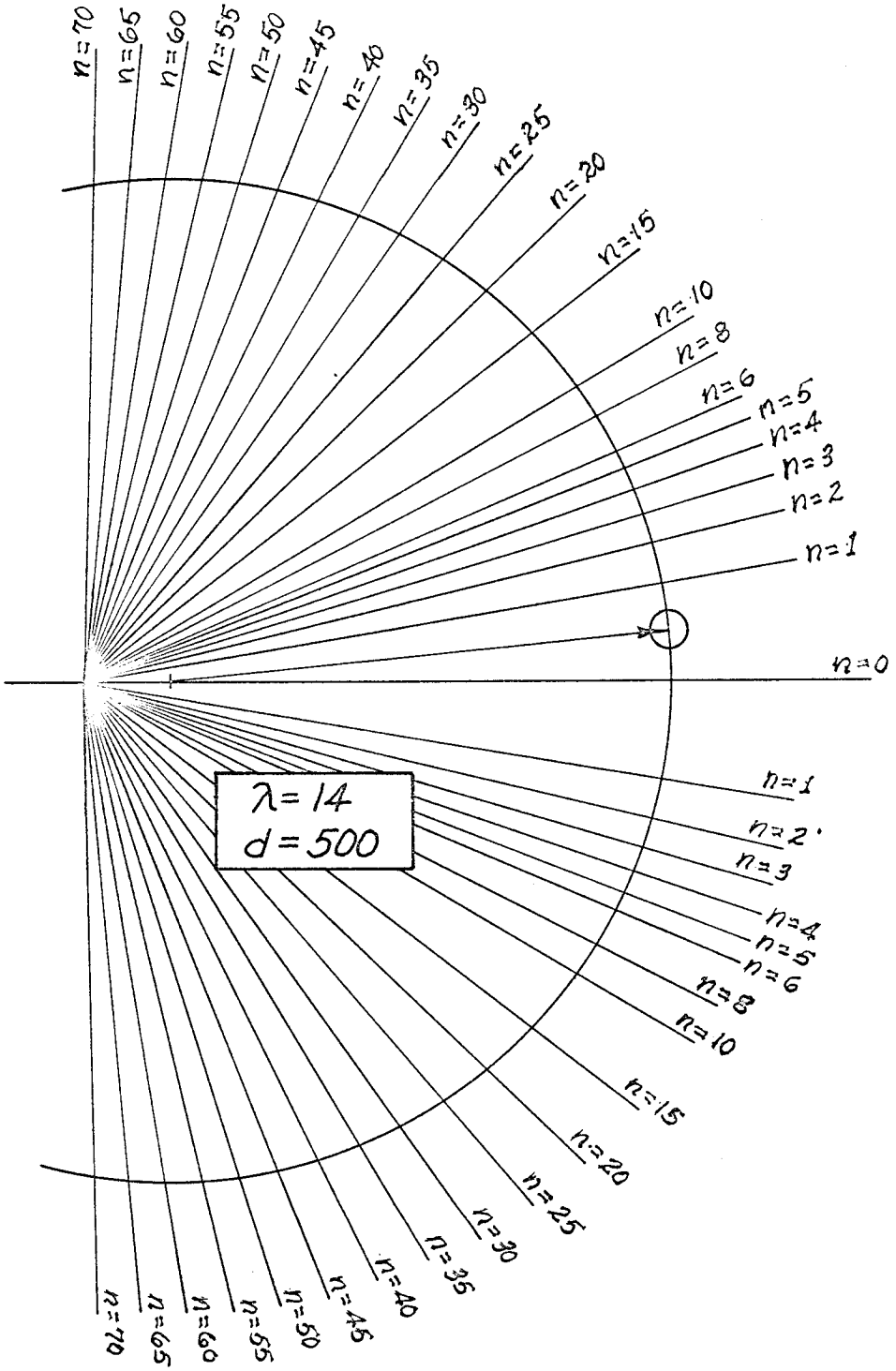

FIG. 6.
CONSTANT PHASE DIFFERENCE CONTOURS

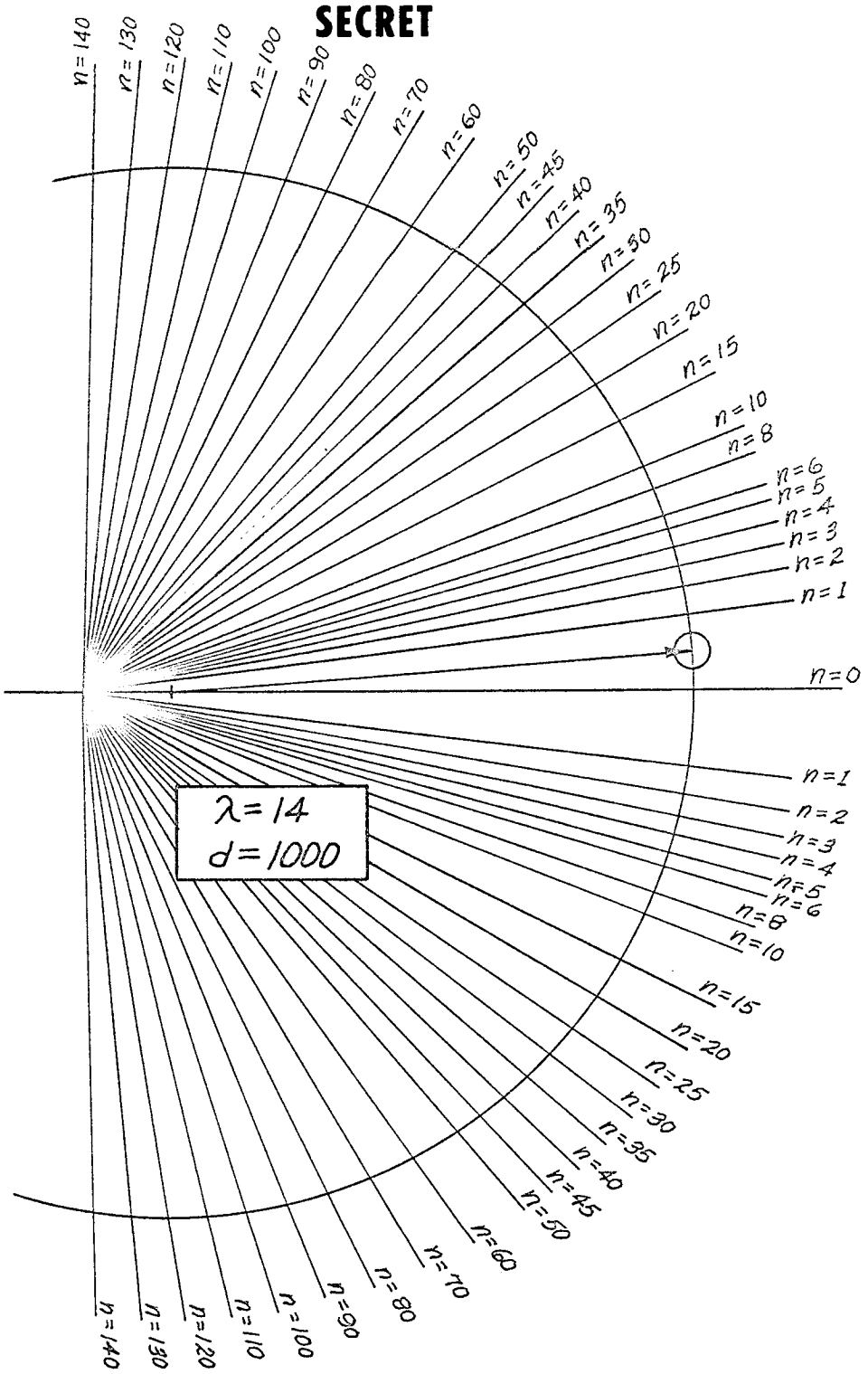

FIG. 7.
CONSTANT PHASE DIFFERENCE CONTOURS

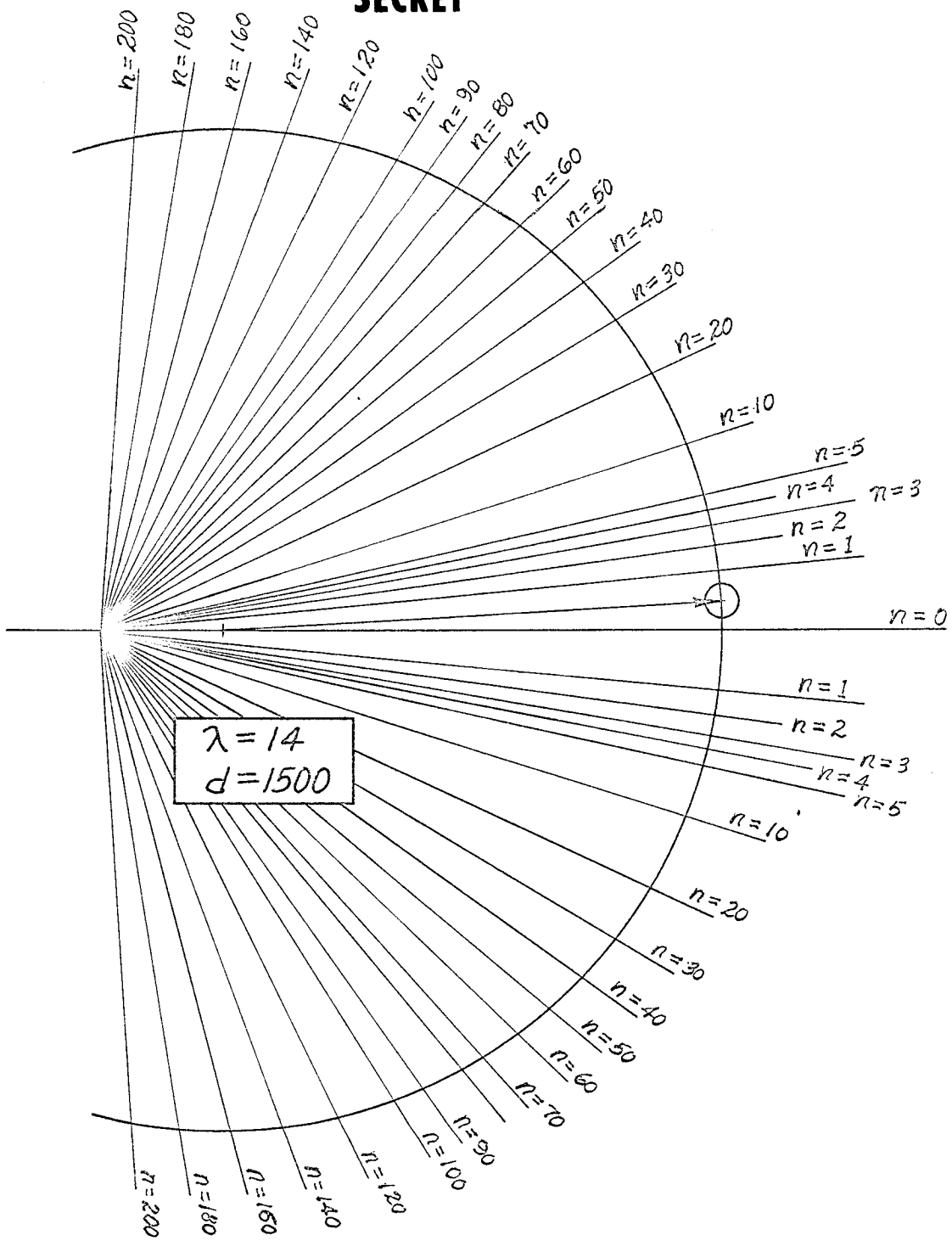

FIG. 8.
CONSTANT PHASE DIFFERENCE CONTOURS

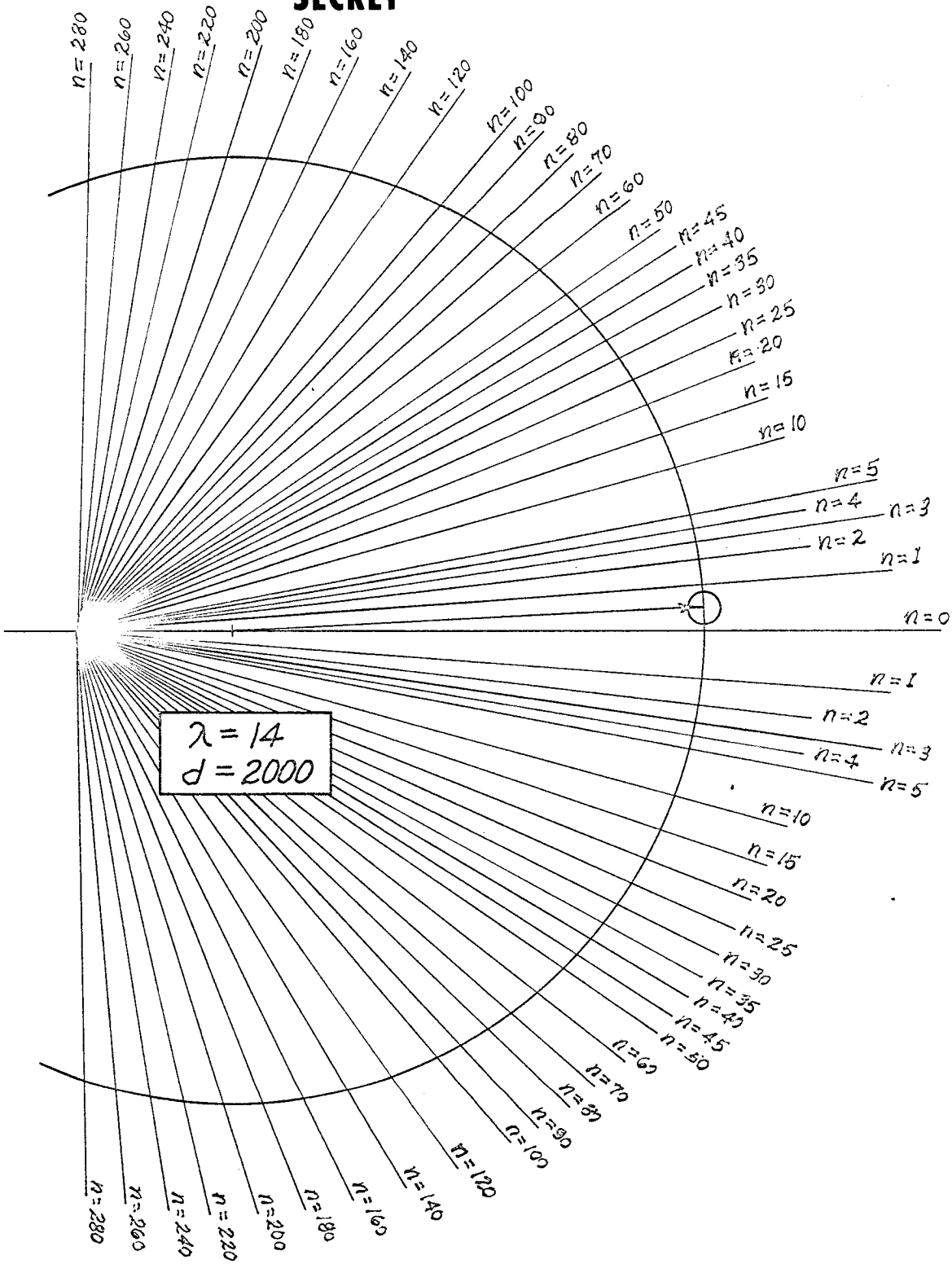

FIG. 9.
CONSTANT PHASE DIFFERENCE CONTOURS

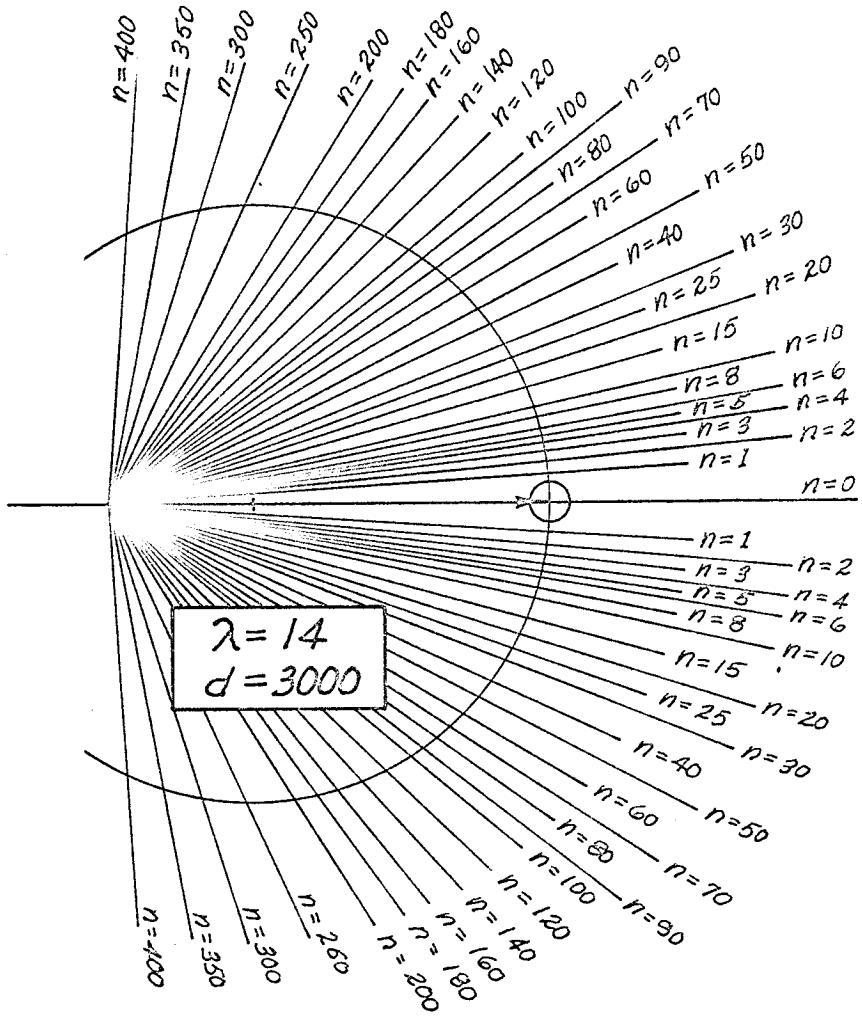

FIG. 10.
CONSTANT PHASE DIFFERENCE CONTOURS

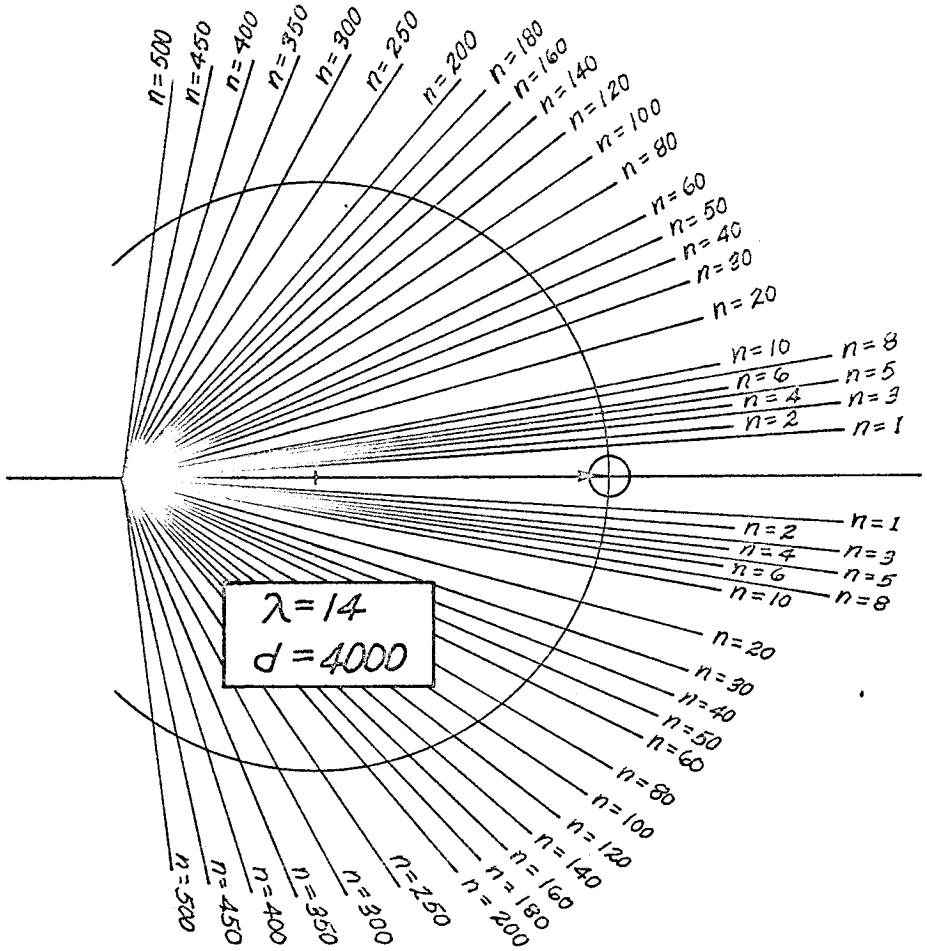

FIG. 11.
CONSTANT PHASE DIFFERENCE CONTOURS

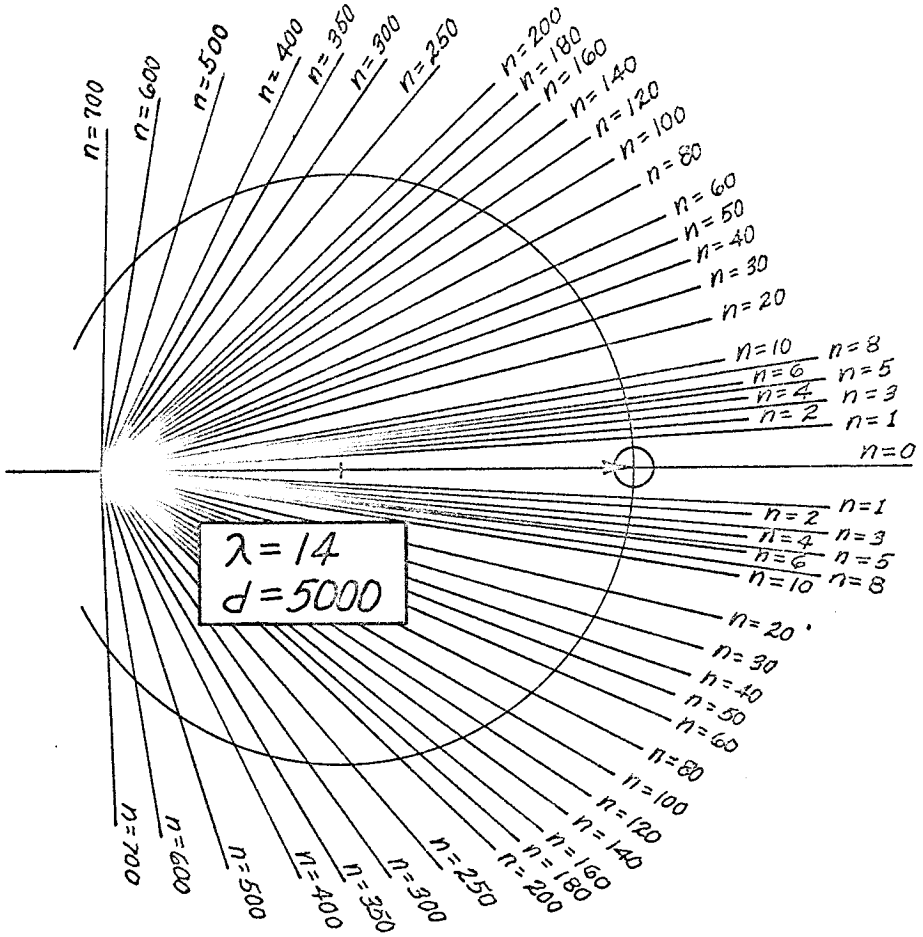

FIG. 12.
CONSTANT PHASE DIFFERENCE CONTOURS

This type of analysis yields a graphical method of obtaining the space pattern of target sensitivity. First, rotate the source about the point R until a given level is obtained; for example, $2/\pi$ (the source just overlapping one region). This establishes the angle α between the source-radar line and the radar-missile line. Mark off the proper distance d on the radar-missile line to obtain one point of the space pattern. Next, go to another set of constant phase contours and repeat the process. A space pattern for a 200-mile diameter source at a distance of 3,000 miles from the radar is shown in Figure 13. The construction line for the $2/\pi$ level at a range of 500 miles is shown in the figure. The pattern width to the 0.637 level increases gradually from a minimum of a little over 200 miles to about 1100 miles at a range of 5,000 miles. The width to the first null varies from about 400 to 1,700 miles.

Referring to the constant phase difference contours, it is seen that the source diameter plays a very important part in determining the pattern width. The width to a given minor lobe level is approximately inversely proportional to the source diameter for higher order lobes, while the main lobe width varies in a more complicated manner. The approximate behavior of the main lobe is shown in Figure 15.

In practice we would not expect to get complete nulls as indicated in the space patterns for two reasons. First, a band of frequencies rather than a single frequency is utilized. Each frequency within the band would have its null at a slightly different spot, thus there would be some filling in of the composite null in wide band systems. Secondly, waves coming in from other weaker sources may fill in the null. (The effect of widely distributed sources are discussed in Section IV of the report.)

Next, we develop an approximate analytical method of determining portions of the space patterns. Rather than rotating the source distribution around R, we rotate it around the point midway between the radar and missile, i.e. the vertex of the asymptotic lines. The source then subtends an angle given by

$$\gamma = \frac{D}{r + d/2} \tag{16}$$

For d much greater than $n\lambda$, the slope of the asymptotes may be represented by

$$\sqrt{\lambda/d\ n} = \tan \theta_n \tag{17}$$

The angle between the two lines is given by

$$B_n = \theta_n - \theta_{n-1} = \tan^{-1}\sqrt{\lambda/d}\ n - \tan^{-1}\sqrt{\lambda/d}\ \sqrt{n-1} \tag{18}$$

$$= \tan^{-1} \frac{\sqrt{\lambda/d}\ (\sqrt{n} - \sqrt{n-1})}{1 + \lambda/d\sqrt{n(n-1)}}$$

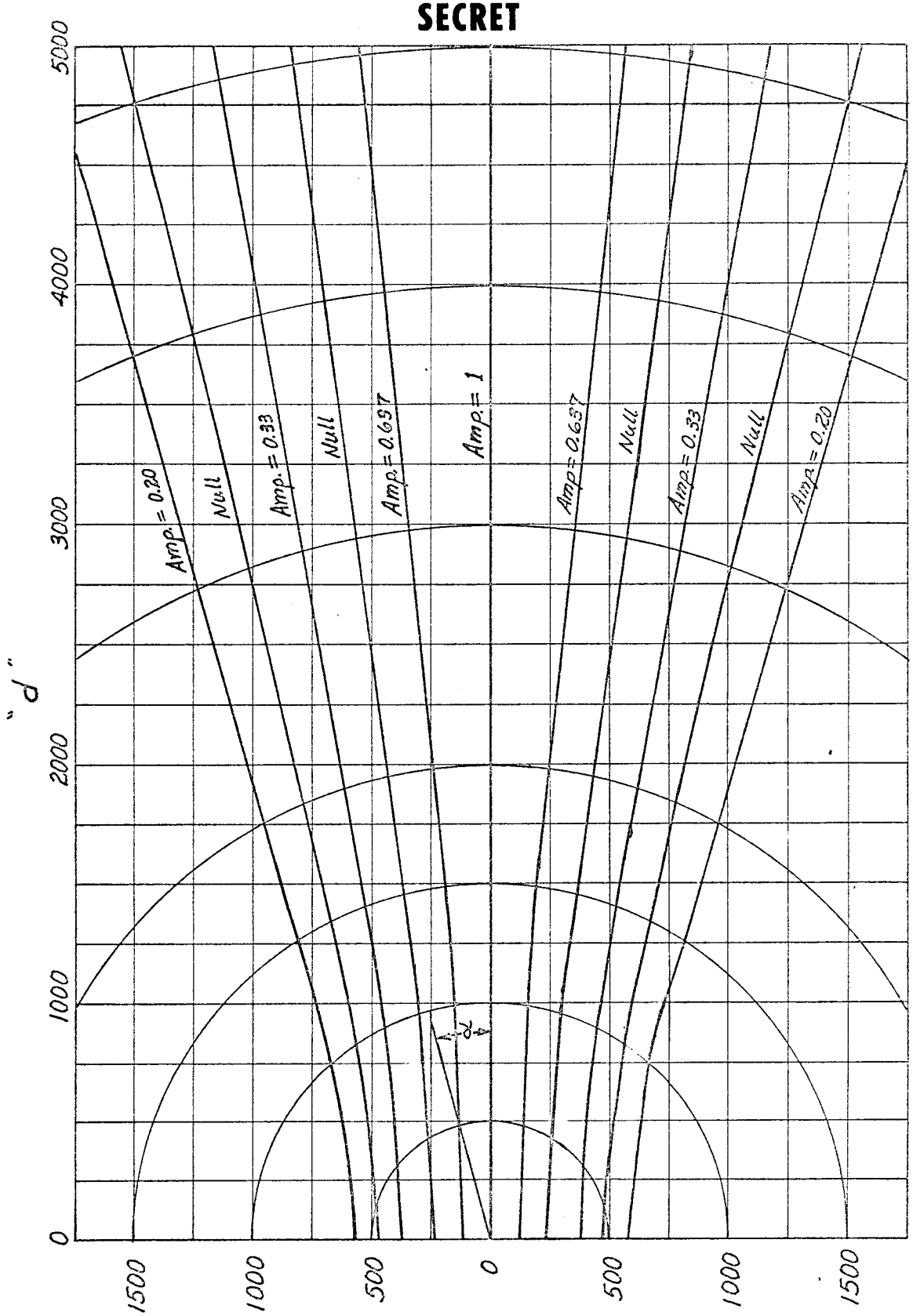

FIG. 13 : SPACE PATTERN : $r = 3000$, $D = 200$

This is approximately equal to

$$Bn = \sqrt{\lambda/d}\ (\sqrt{n} - \sqrt{n-1} \tag{19}$$

for small angles. The $2/\pi$ amplitude contour line numbers are obtained by equating (16) and (19) to give

$$\sqrt{n} - \sqrt{n-1} = \sqrt{d/\lambda}\ \frac{D}{r + d/2} \tag{20}$$

The pattern will have nulls when

$$Bn = 1/2\rho \checkmark = 1/2\rho\ \frac{D}{r + d/2} \quad \rho = 1, 2 \ldots\ldots \tag{21}$$

and minor lobes of amplitude $1/2\rho + 1$ when

$$Bn = 1/2\rho + 1 \checkmark \quad \rho = 1, 2 \ldots\ldots \tag{22}$$

or

$$\sqrt{n} - \sqrt{n-1} = 1/2\rho + 1\ \sqrt{d/\lambda}\ \frac{D}{r + d/2} \tag{23}$$

We denote the slope of the particular line satisfying equation (20) or (23) as

$$\tan \theta_N = \sqrt{\lambda/2\ N} \tag{24}$$

Next we relate this to the pattern width. Referring to Figure 14 below, we see that the width is given by

$$W = 2d \sin \alpha \tag{25}$$

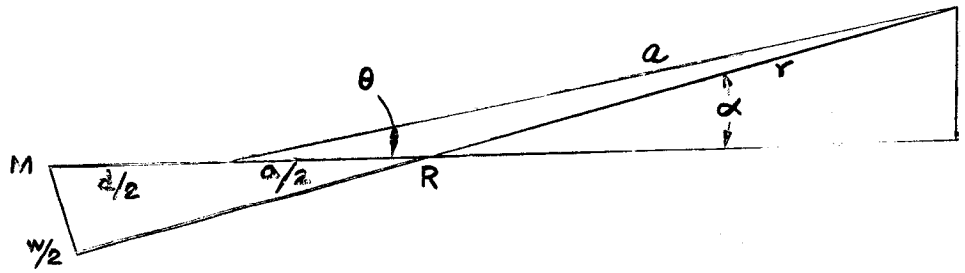

Figure 14.

We also see that

$$\sin \alpha = a/r \sin \theta$$

$$= \frac{r + d/2}{r} \sin \theta = \frac{r + d/2}{r} \tan \theta \tag{26}$$

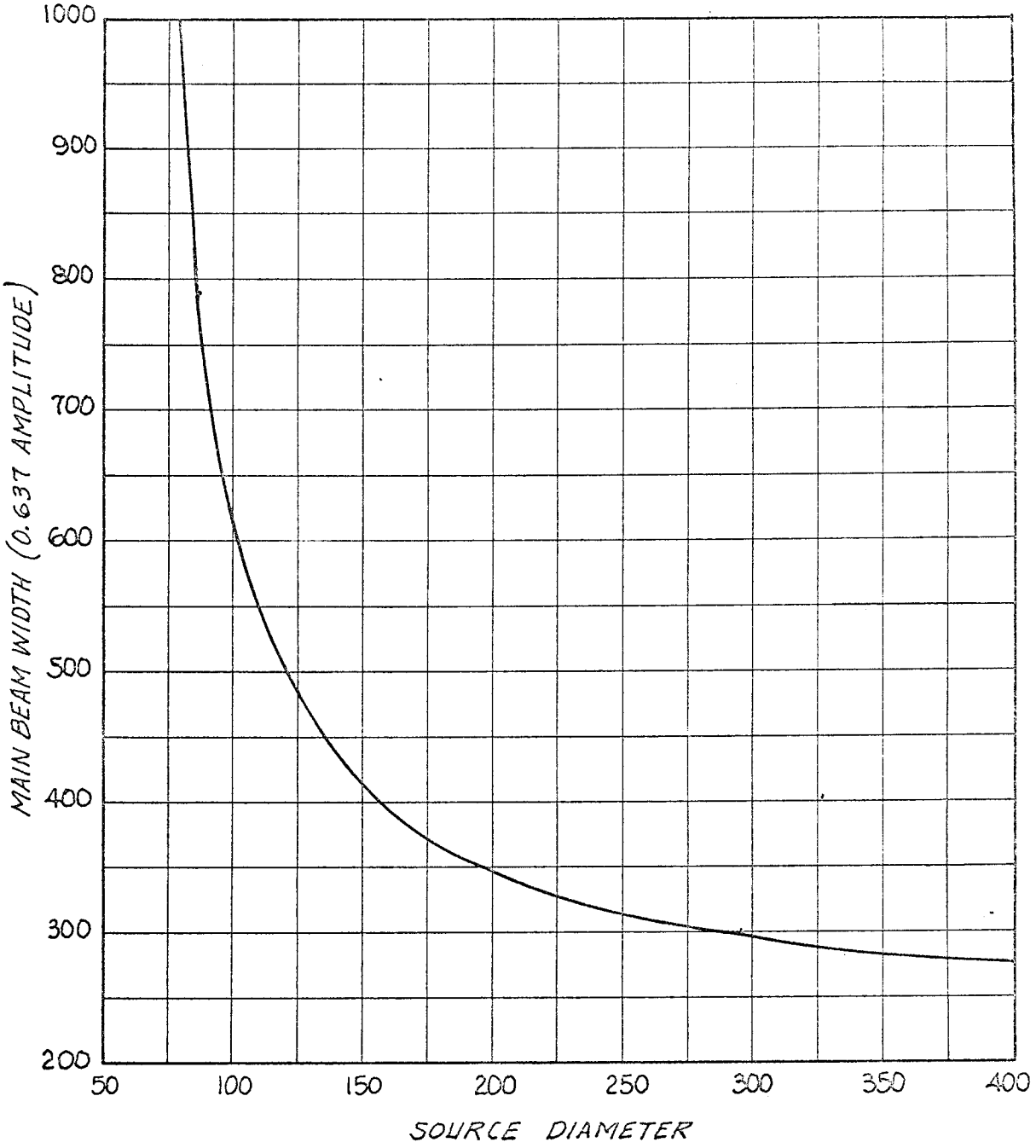

FIG. 15.

PATTERN WIDTH vs. SOURCE SIZE FOR r = 3000, d = 1000

for small values of θ. Combining equations (24), (25), and (26), we obtain

$$W = 2\,\frac{r + d/2}{r}\,\sqrt{n\lambda d} \qquad (27)$$

where N is a solution to equation (20) or (23). We make use of equation (27) to obtain Figure 15, which shows pattern width versus source diameter for a source range of 3,000 miles and a target range of 1,000 miles.

IV. WIDELY DISTRIBUTED SOURCES

In this section, we consider low level signals coming in uniformly from all directions. This situation might be caused by widely scattered storms at great distances. The contribution of a source to the trail back scatter will be proportional to the angle it subtends. Making use of equation (19) we see that the signal will be given by

$$S = K\left[A_1\sqrt{1} - A_2\,(\sqrt{2}-\sqrt{1}) + A_3\,(\sqrt{3}-\sqrt{2}) - A_4\,(\sqrt{4}-\sqrt{3}) + \ldots\right] \qquad (28)$$

where the A terms are the magnitudes of the various lobes of the range function. If all terms are equal, we see that the resulting signal is always greater than the signal resulting from the first two regions or 0.59 of the signal originating from the first region since the regions are decreasing monotonically in size. It is also noted that, regardless of the number of regions utilized, the resulting signal will always be less than that resulting from the first region alone. Arbitrarily chosing ten and eleven regions for consideration, we find that the resulting magnitude is between 0.70 and 0.85 of the first region contribution.

V. IMPLICATIONS OF RESULTS

In selecting monitoring sites, it should be borne in mind that maximum sensitivity will occur for targets which are in line with the source and radar. For detection of targets outside the main beam, it would be desirable to use two radars operating on different frequencies so that the null, or reduced sensitivity regions of the first radar, could be covered by the second.

Since the source size determines the pattern width, there is an urgent need to determine the size and distribution of sources suitable for scatter measurements on domestic and foreign launches. This could be done by utilizing crossed loop direction finding apparatus located so that the source subtends a fairly large angle. Usable measuring sites would be selected as a function of the source size and direction finder resolution. At the present time, the best estimates of source size and location are obtained from atmospheric noise contour data. Existing data plots show the contours as if the time were the same over the whole earth. This data is useful for nondirectional receiving systems; however, for directional systems, it is desirable to know the direction of arrival of energy from strong sources. To help satisfy this need, real time atmospheric noise contours are presented in the Appendix.

One of the primary purposes of a directive receiving antenna is to reduce the effects of stray reflections outside the region of interest. Since the space pattern can be represented as a directional pattern at a specific range as far as reflections are concerned, it will have an important effect on antenna design considerations. Effective antenna patterns (assuming a monopole receiving antenna) for 500 and 3,000-mile ranges are shown in Figure 16 and 17. In both of these cases, the source is assumed to be 200 miles in diameter and located 3,000 miles from the radar. Only the forward portion of the pattern is shown. In general, the back portion will be similar but narrower. The "effective" antenna pattern would be multiplied by the receiving antenna pattern to obtain the resulting response to reflectors. As far as antenna noise pickup is concerned, only the receiving antenna pattern should be considered.

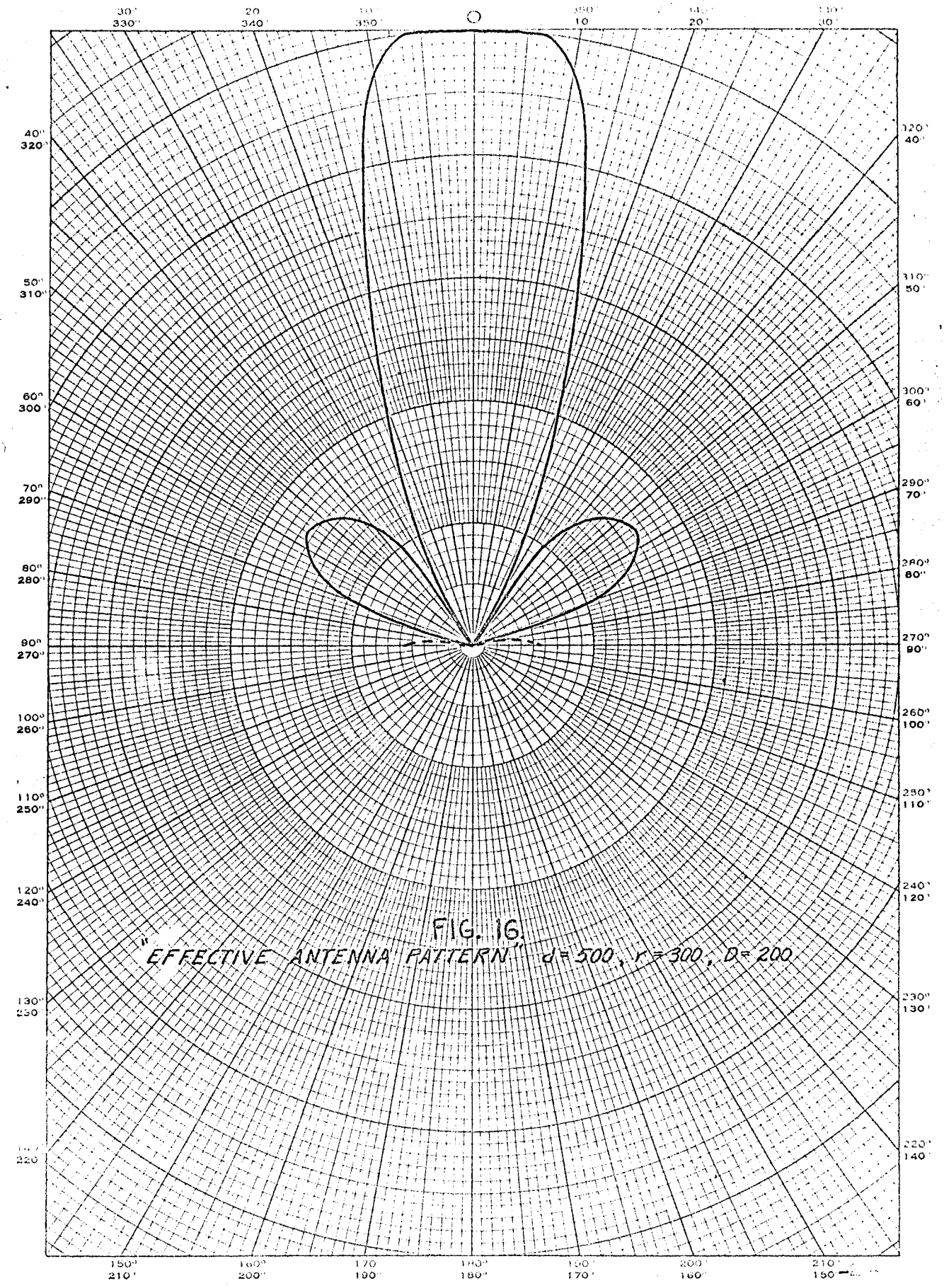

FIG. 16.
"EFFECTIVE ANTENNA PATTERN" d = 500, r = 300, D = 200.

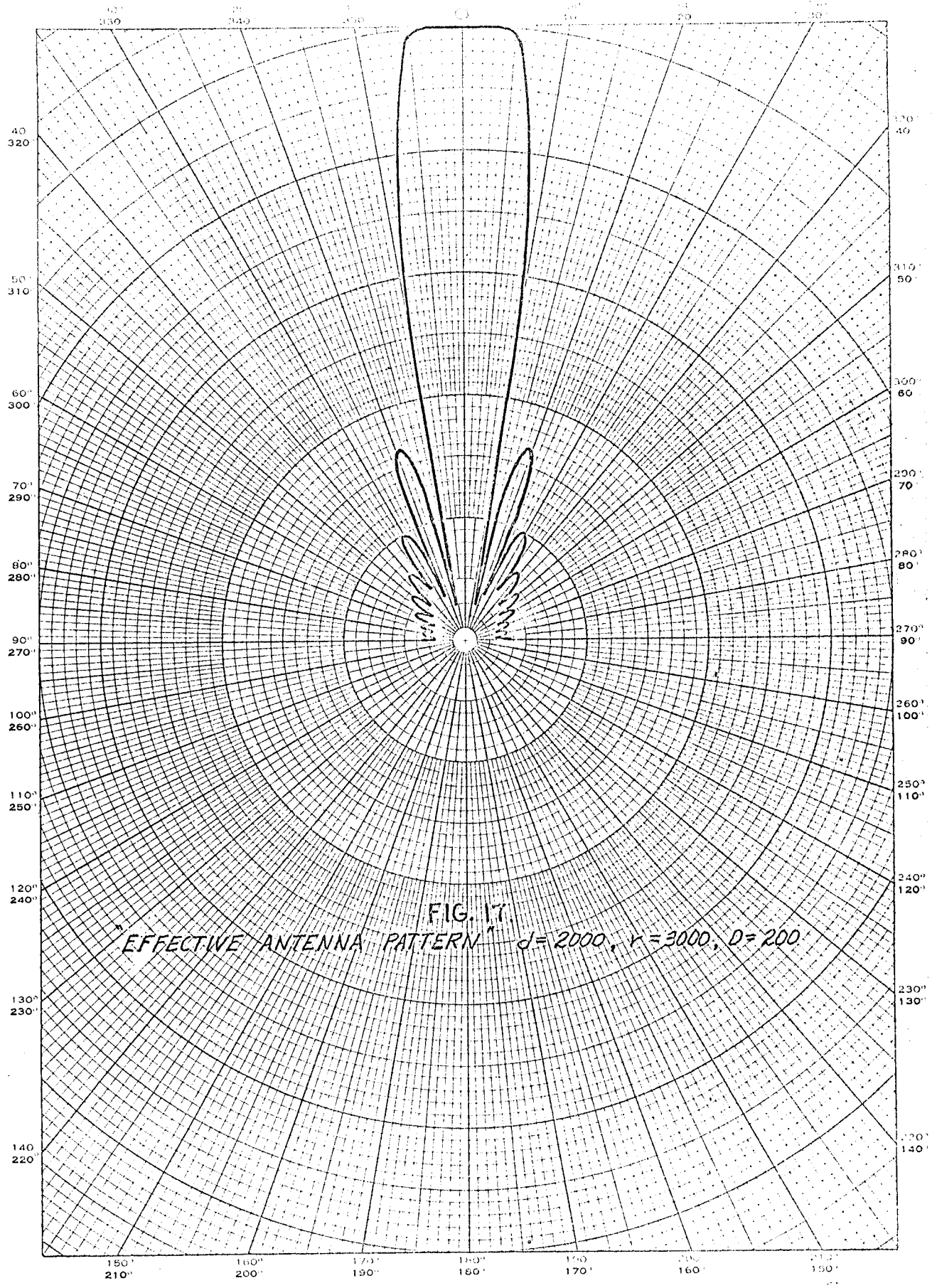

FIG. 17

"EFFECTIVE ANTENNA PATTERN" d = 2000, Y = 3000, D = 200

APPENDIX

REAL TIME ATMOSPHERIC NOISE CONTOURS

by

D. L. Caudill

APPENDIX

Existing noise contours are plotted as if the time over the whole earth were the same. This data is useful for non-directional receiving systems; however, for directional systems, it is desirable to know the strength and direction of arrival of waves from the various sources. To aid in this, real time atmospheric noise contours are presented.

Figures 18 to 41, inclusive, are charts showing the estimated median values of noise in db above 1 uv/m at a frequency of 20 kc/s that occur simultaneously over the world at any given time. The charts cover the day in 4-hour time blocks (Greenwich Time) and the year by 3-month periods (the four seasons), making a total of 24 charts.

At the points of greatest change in propagation conditions (sunrise and sunset), the curves represent a certain amount of interpolation; but, in any case, they appear to represent the noise variations as well as is justified by the data available at present.

Noise values at frequencies other than 20 kc/s can be derived by the use of Figure 42.

All data used for Figures 18 through 42 was obtained from "Revision of Atmospheric Radio Noise Data", International Radio Consultative Committee, Report No. 65. 1957.

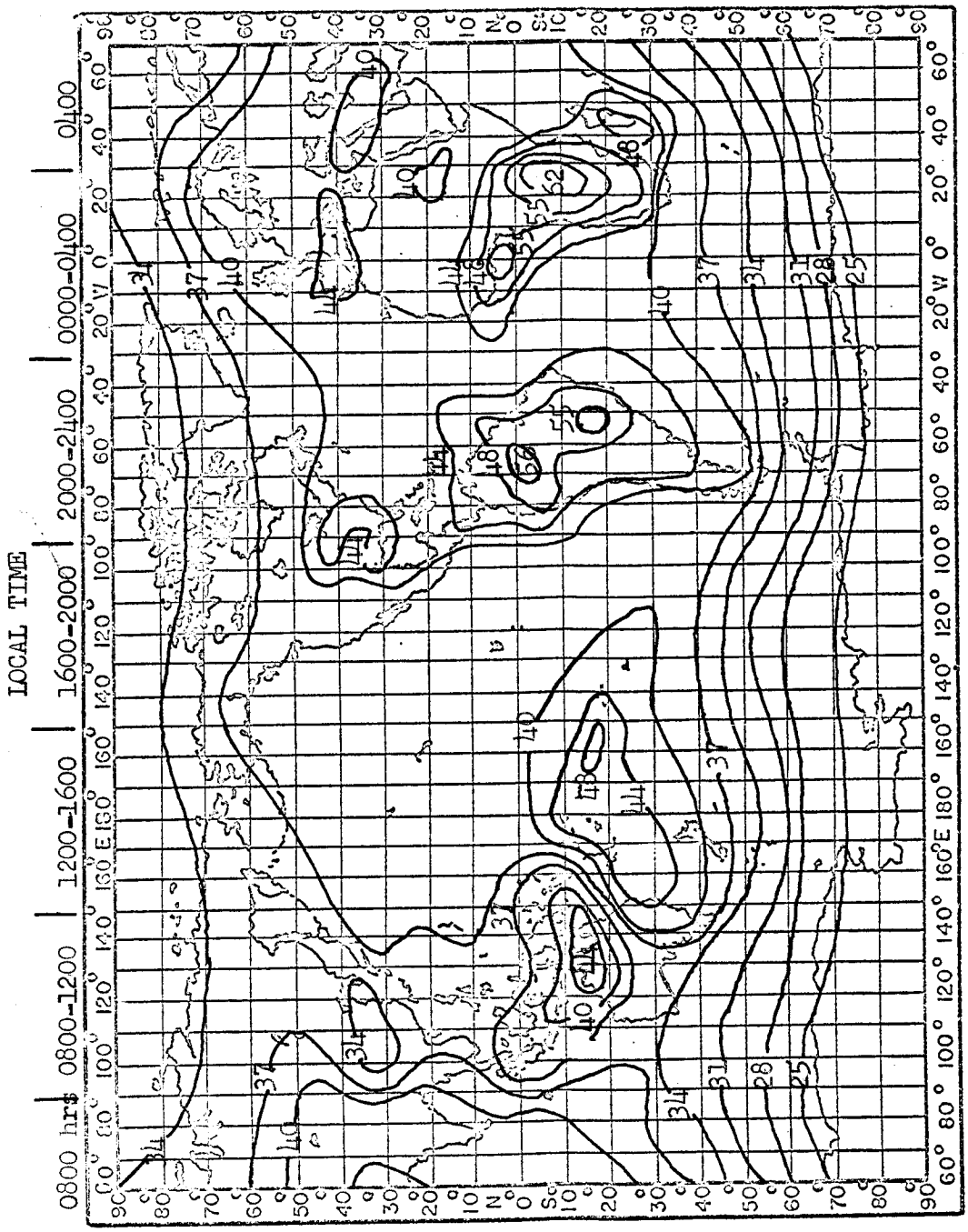

Figure 18. Expected values of radio noise (in db above 1 uv/m for 1 kc/s bandwidth) at 20 kc/s, from 0000-0400 hrs. Greenwich Time, for December, January, February.

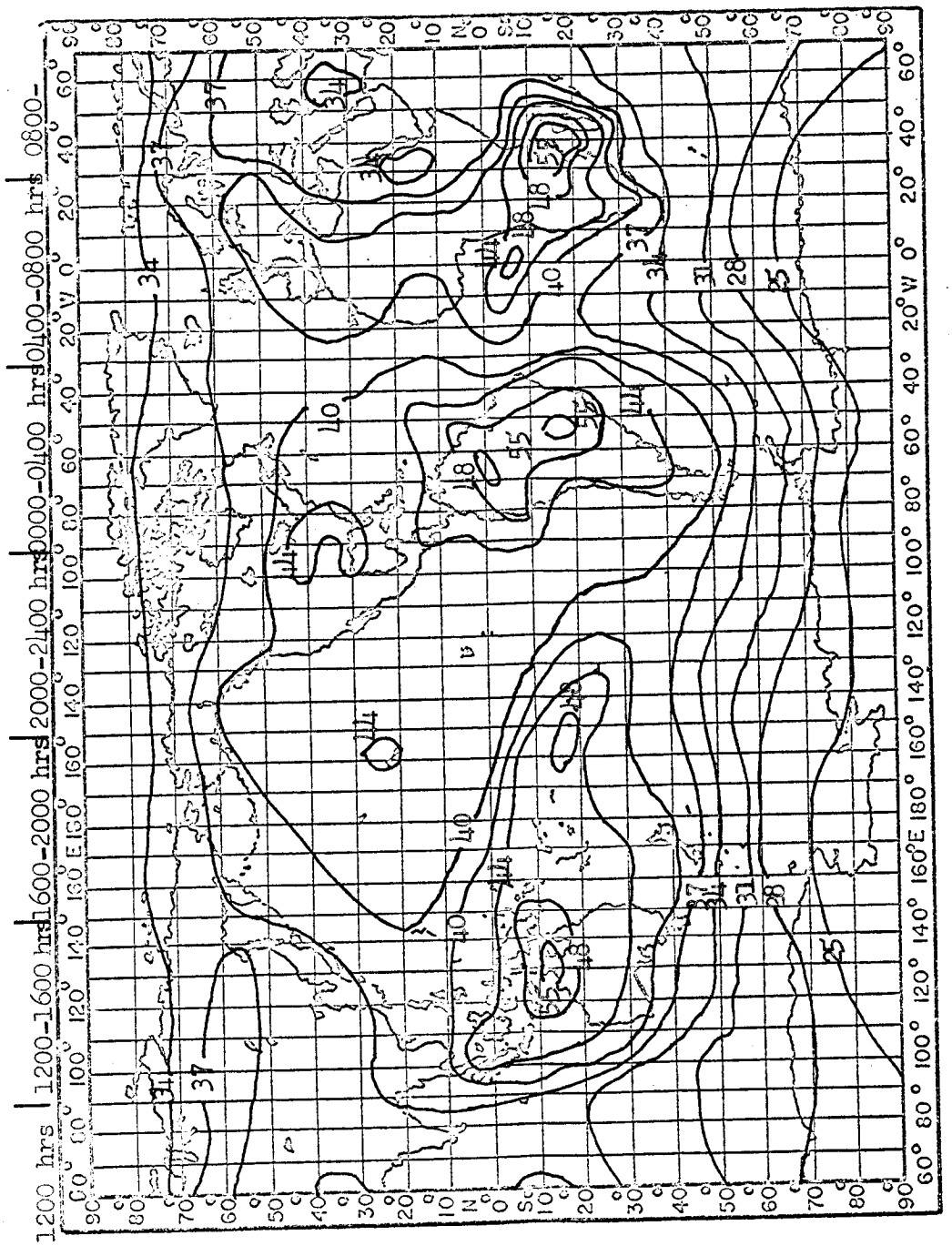

Figure 19. Expected values of radio noise (in db above 1 uv/m for 1 kc/s bandwidth) at 20 kc/s, from 0400-0800 hrs Greenwich Time, for December, January, February.

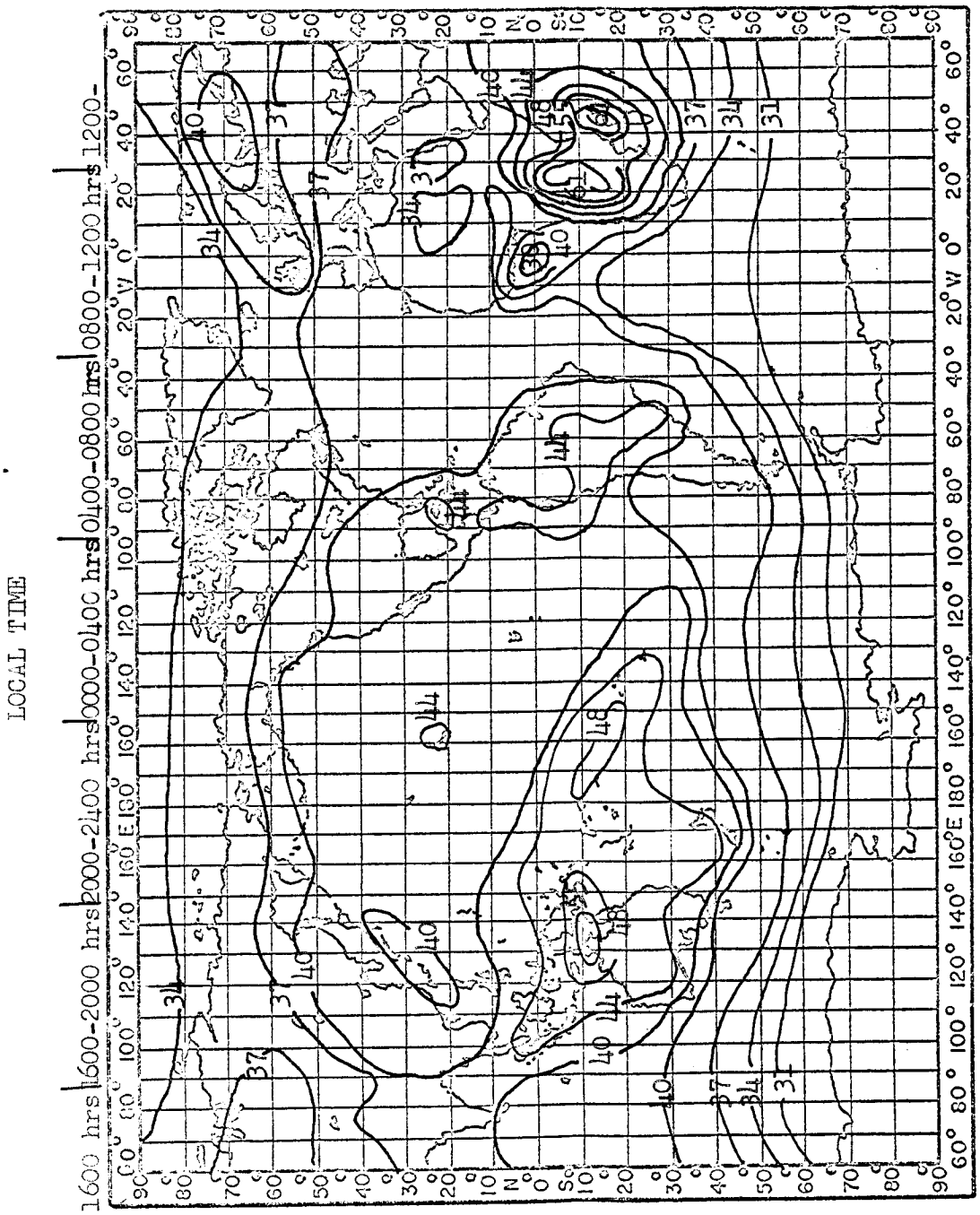

Figure 20. Expected values of radio noise (in db above 1 uv/m for 1 kc/s bandwidth) at 20 kc/s, from 0800-1200 hrs Greenwich Time, for December, January, February.

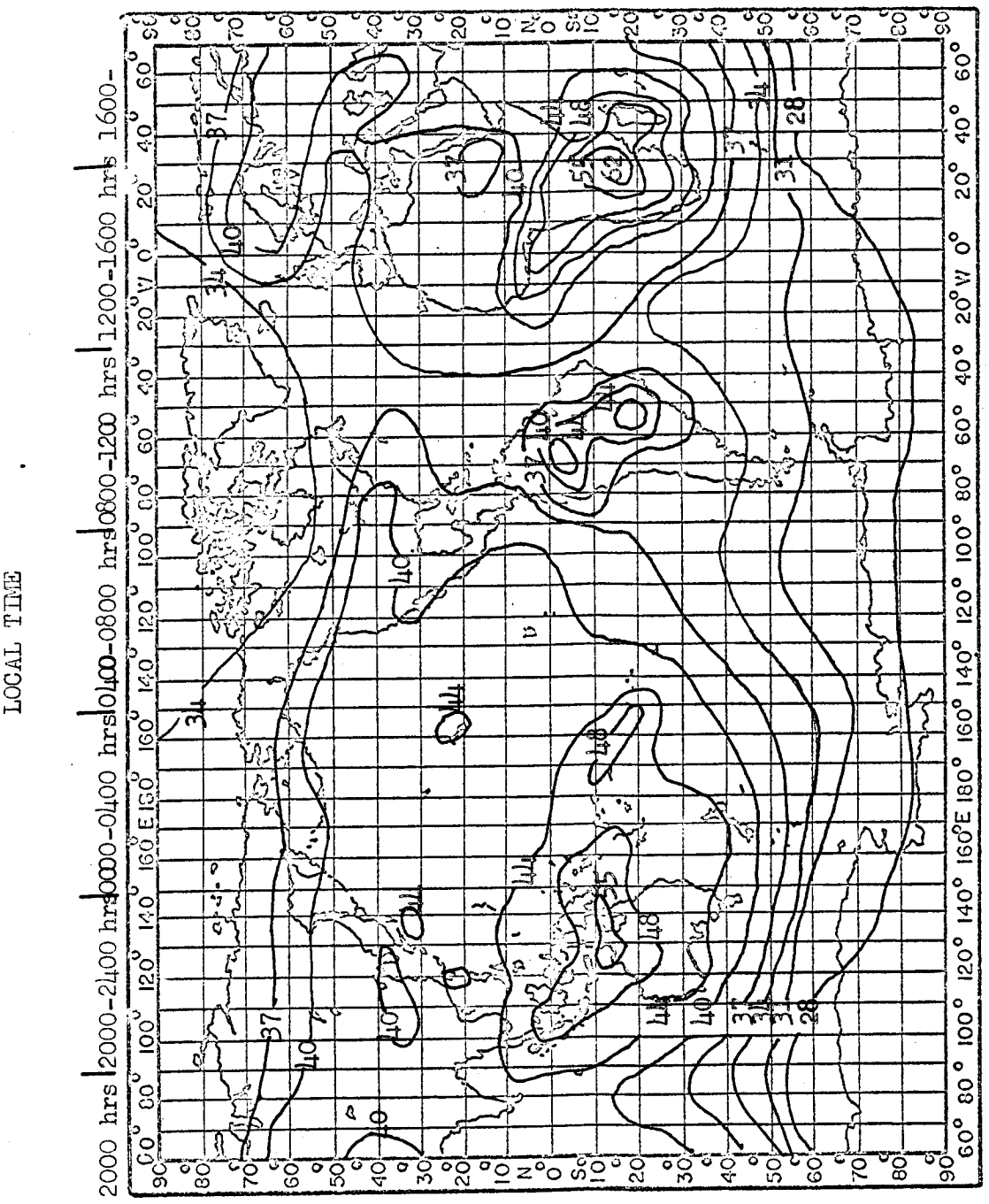

Figure 21. Expected values of radio noise (in db above 1 uv/m for 1 kc/s bandwidth) at 20 kc/s, from 1200-1600 hrs. Greenwich Time, for December, January, February.

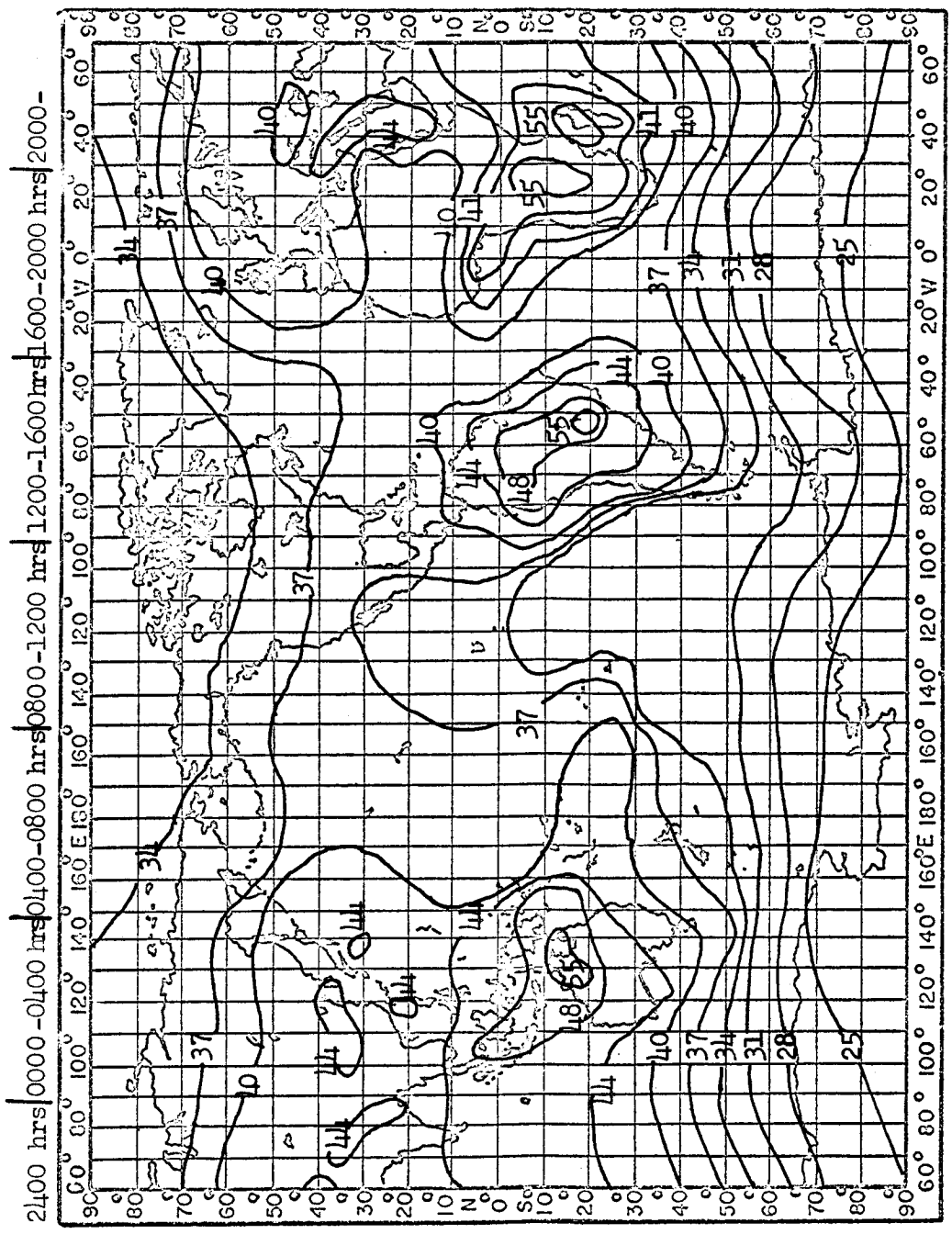

Figure 22. Expected values of radio noise (in db above 1 uv/m for 1 kc/s bandwidth) at 20 kc/s, from 1600-2000 hrs. Greenwich Time, for December, January, February.

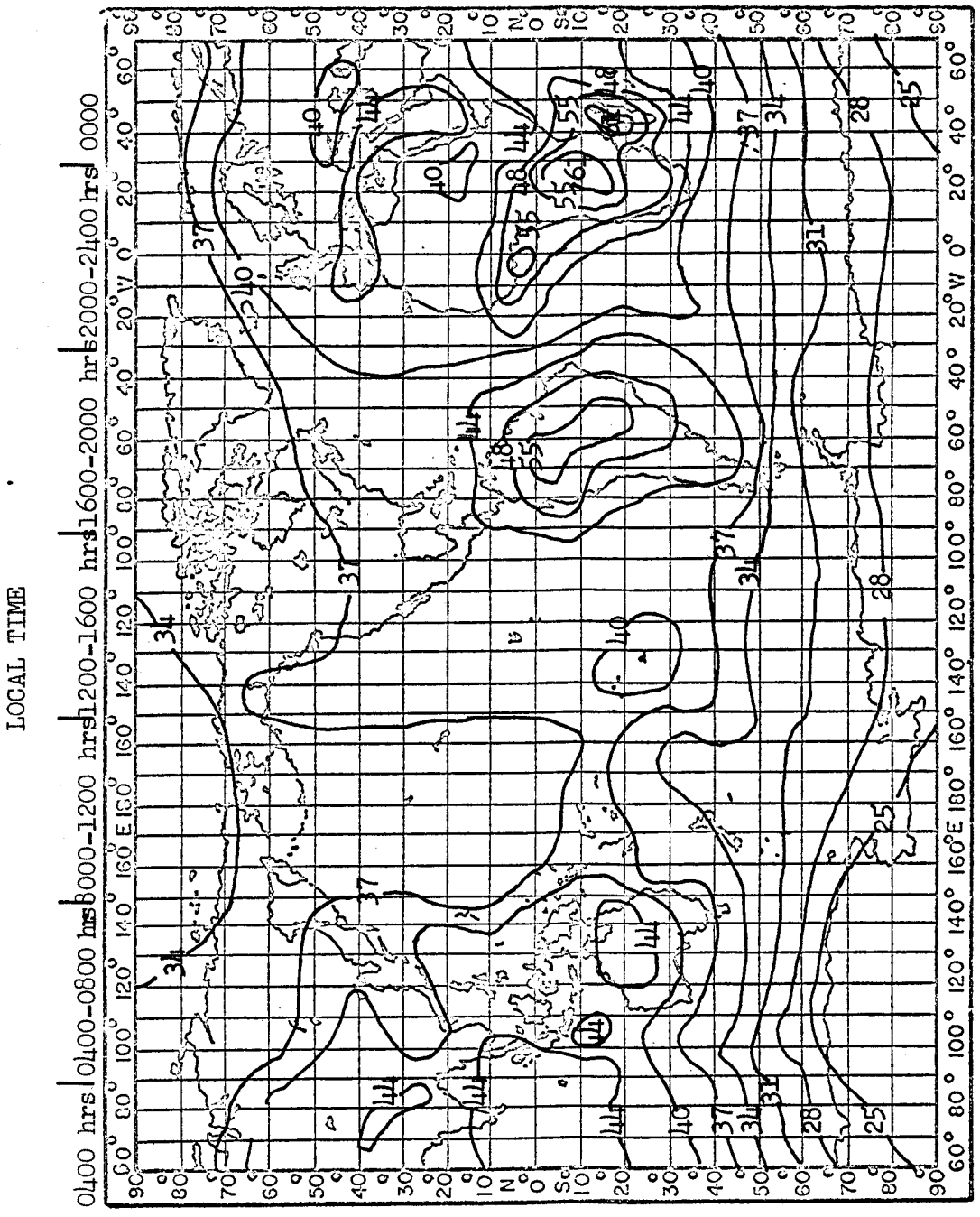

Figure 23. Expected values of radio noise (in db above 1 uv/m for 1 kc/s bandwidth) at 20 kc/s, from 2000-2400 hrs. Greenwich Time, for December, January, February.

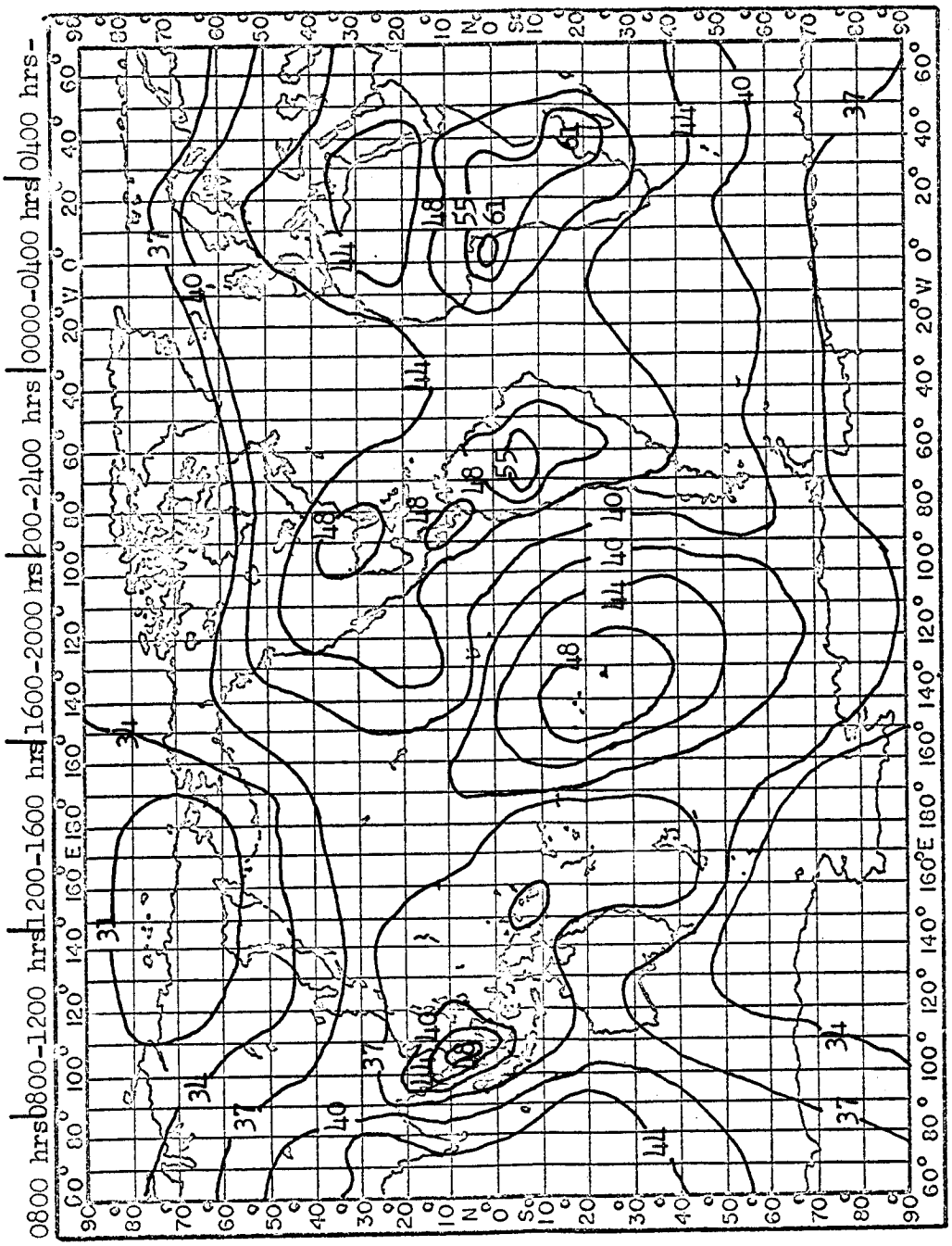

Figure 24. Expected values of radio noise (in db above 1 uv/m for 1 kc/s bandwidth) at 20 kc/s, from 000-0400 hrs. Greenwich Time, for March, April, May.

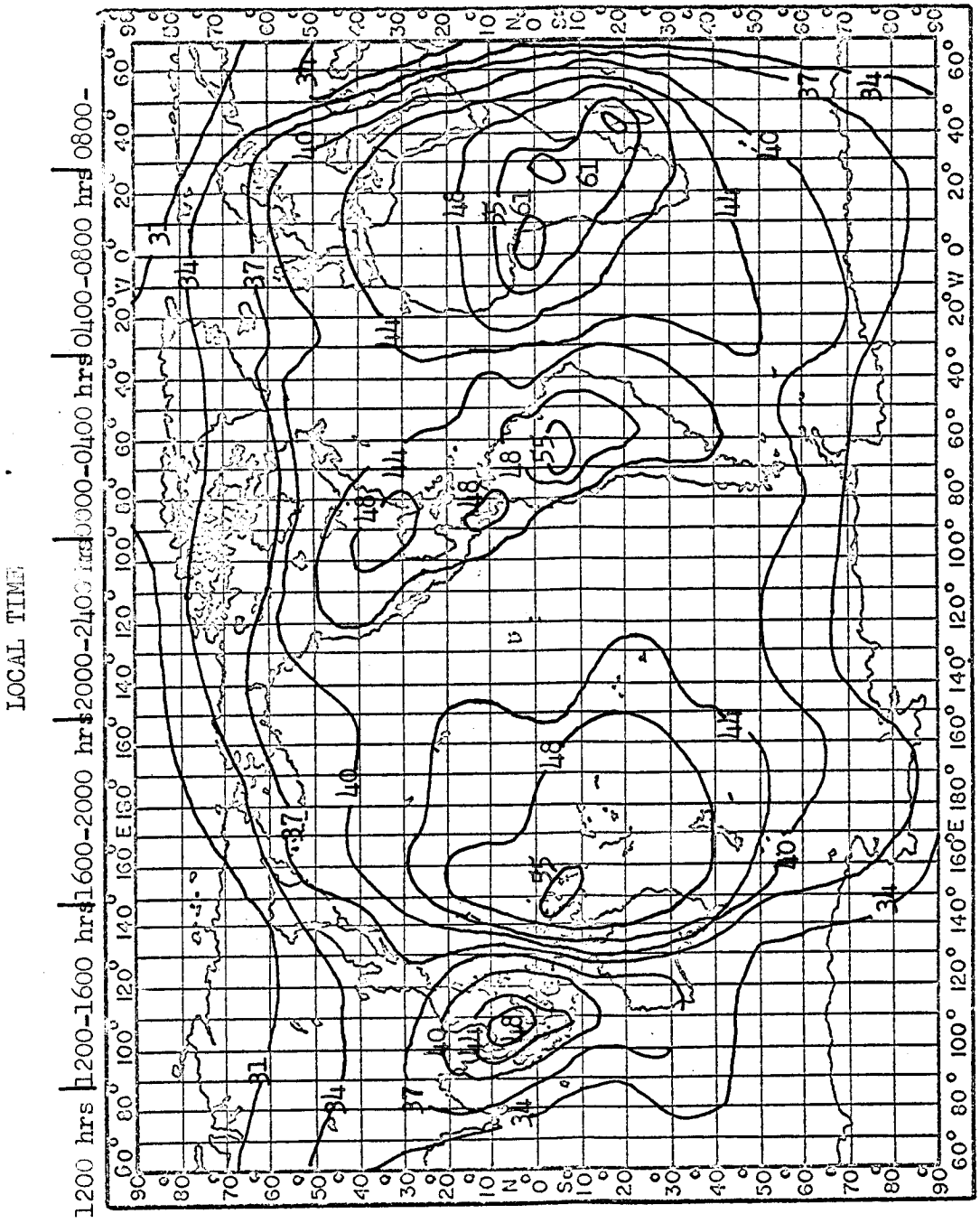

Figure 25. Expected values of radio noise (in db above 1 uw/m for 1 kc/s bandwidth) at 20 kc/s, from 0400-0800 hrs. Greenwich Time, for March, April, May.

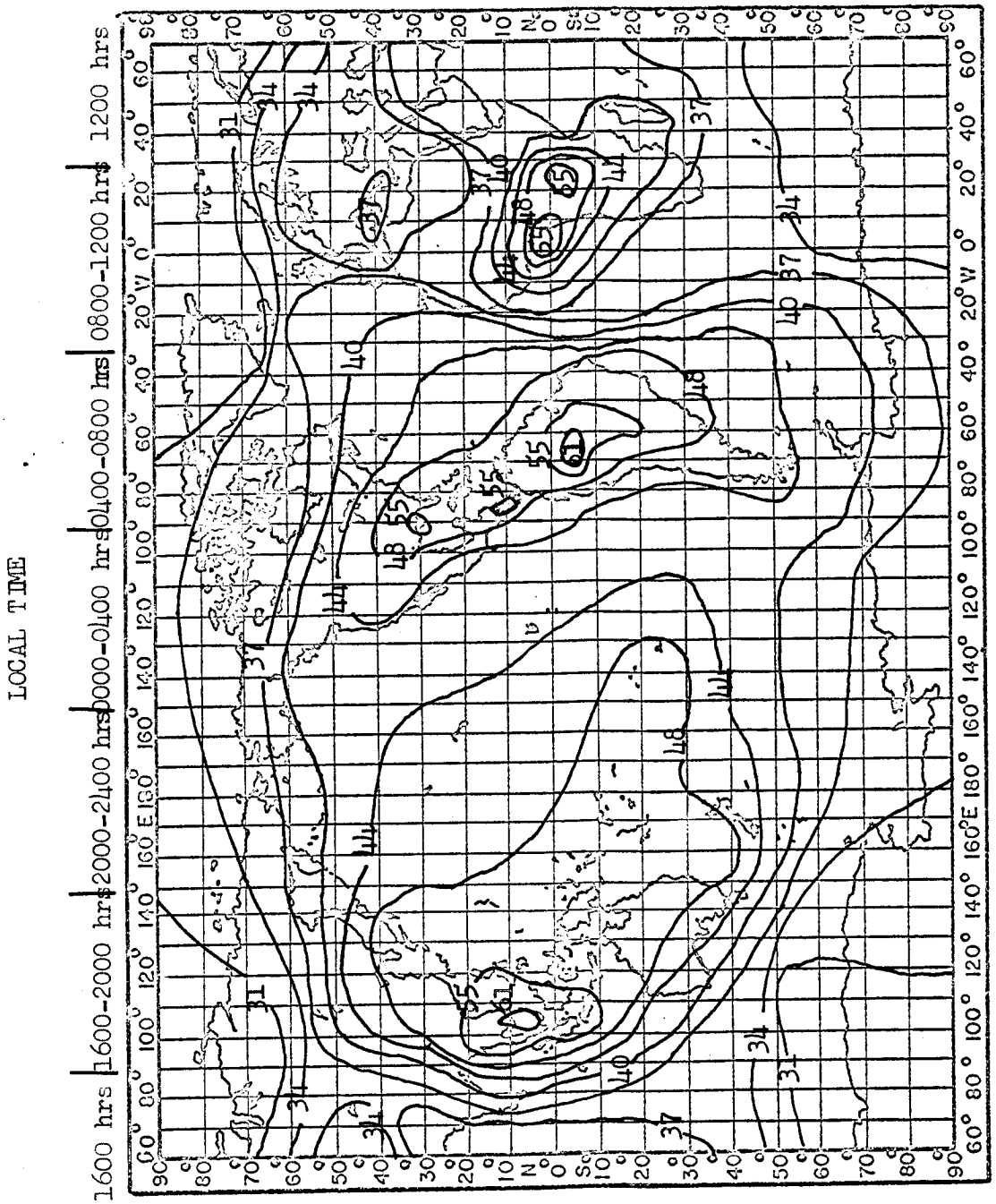

Figure 26. Expected values of radio noise (in db above 1 uv/m for 1 kc/s bandwidth) at 20 kc/s, from 0800-1200 hrs. Greenwich Time, for March, April, May.

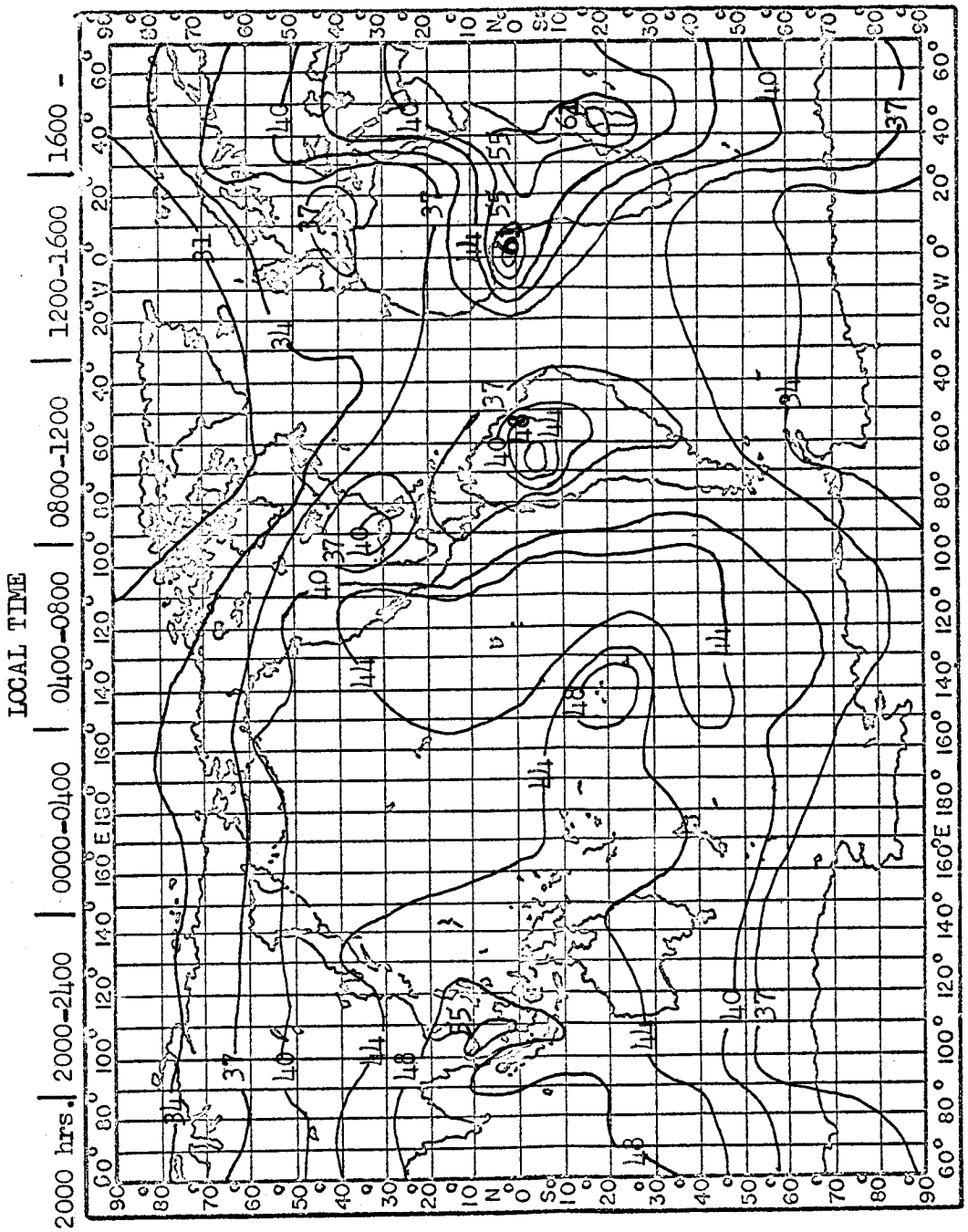

Figure 27. Expected values of radio noise (in db above 1 uv/m for 1 kc/s bandwidth) at 20 kc/s, from 1200-1600 hrs. Greenwich Time, for March, April, May.

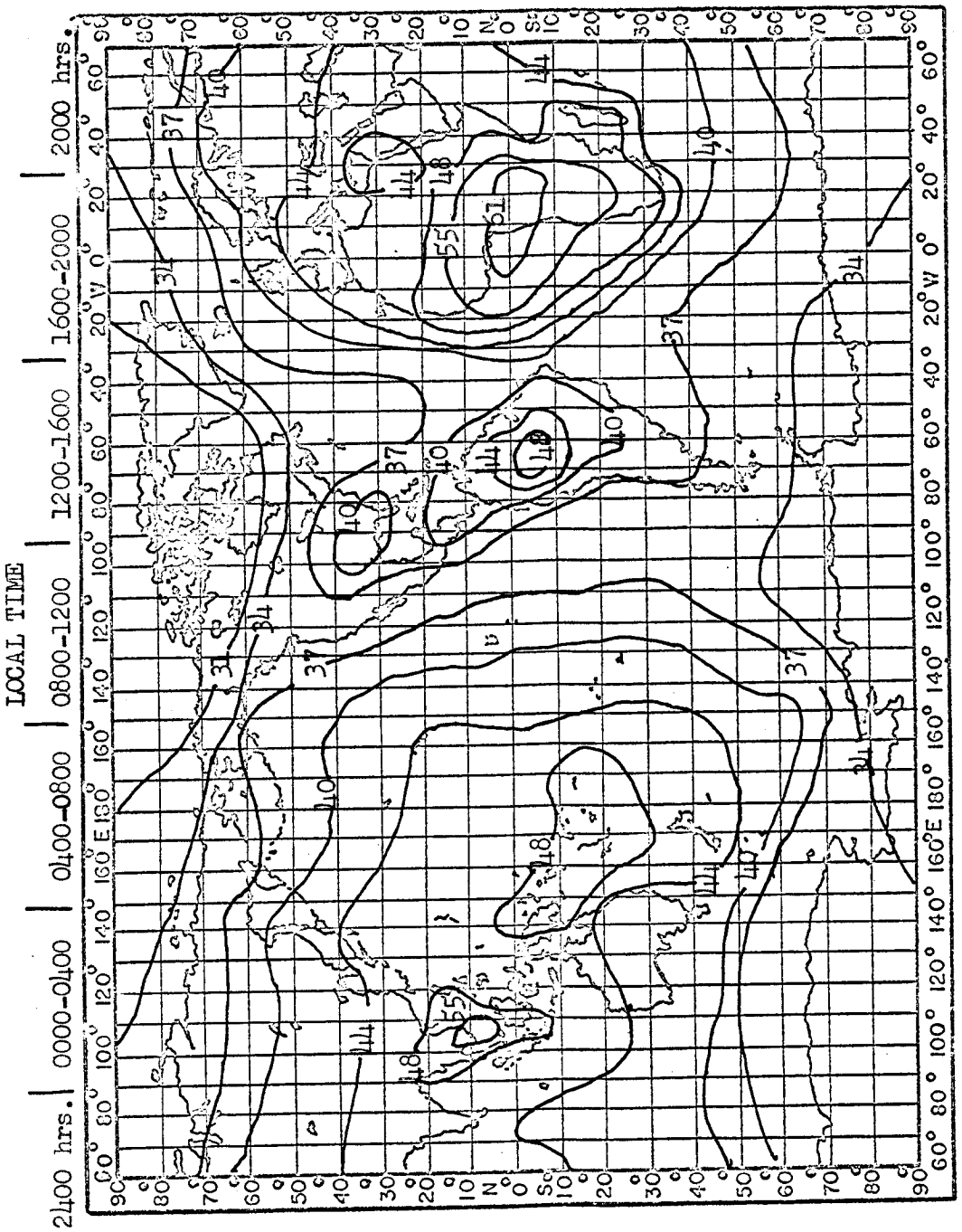

Figure 28. Expected values of radio noise (in db above 1 uv/m for 1 kc/s bandwidth) at 20 kc/s, from 1600-2000 hrs. Greenwich Time, for March, April, May.

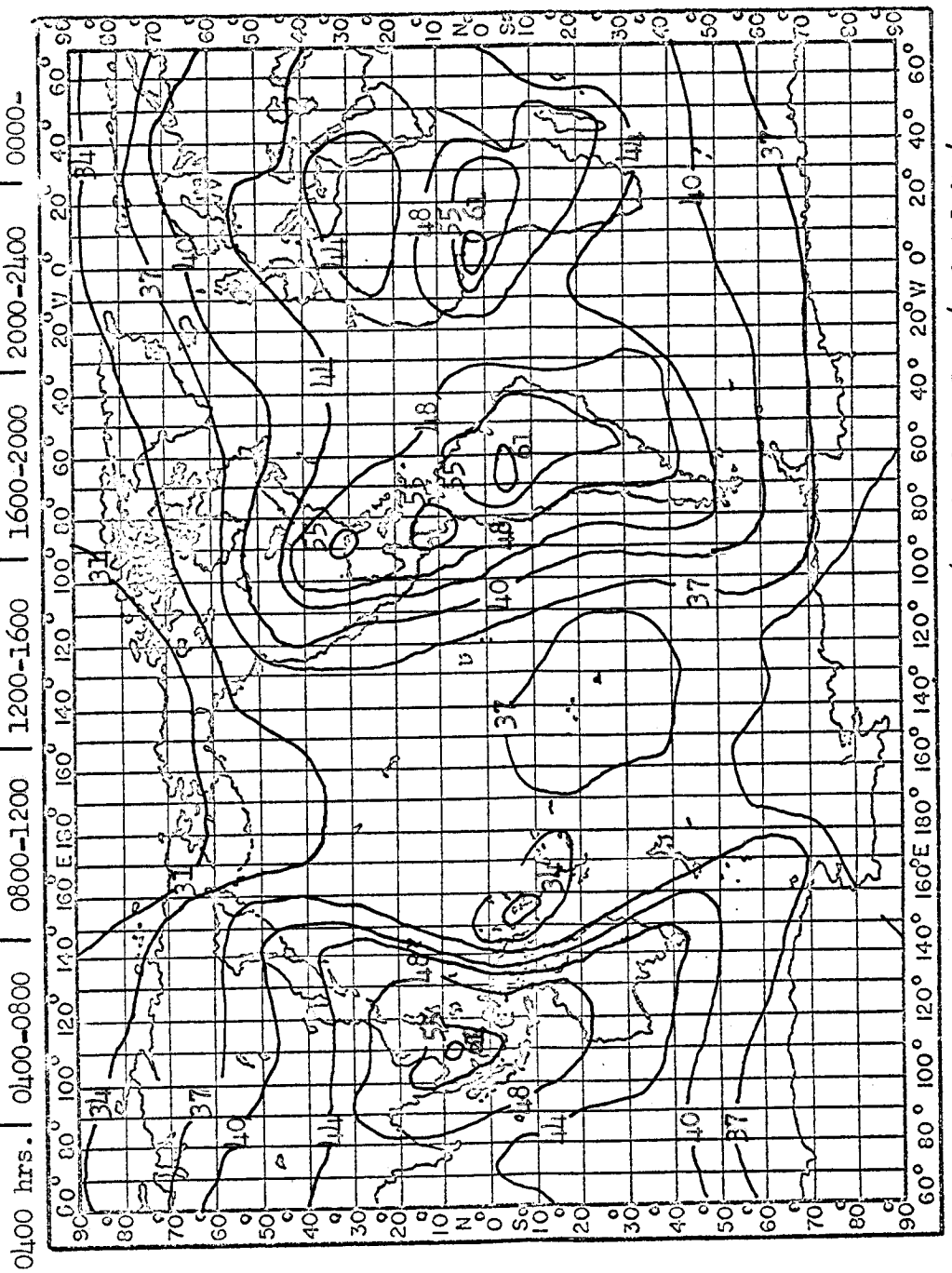

Figure 29. Expected values of radio noise (in db above 1 uv/m for 1 kc/s bandwidth) at 20 kc/s, from 2000-2400 hrs. Greenwich Time, for March, April, May.

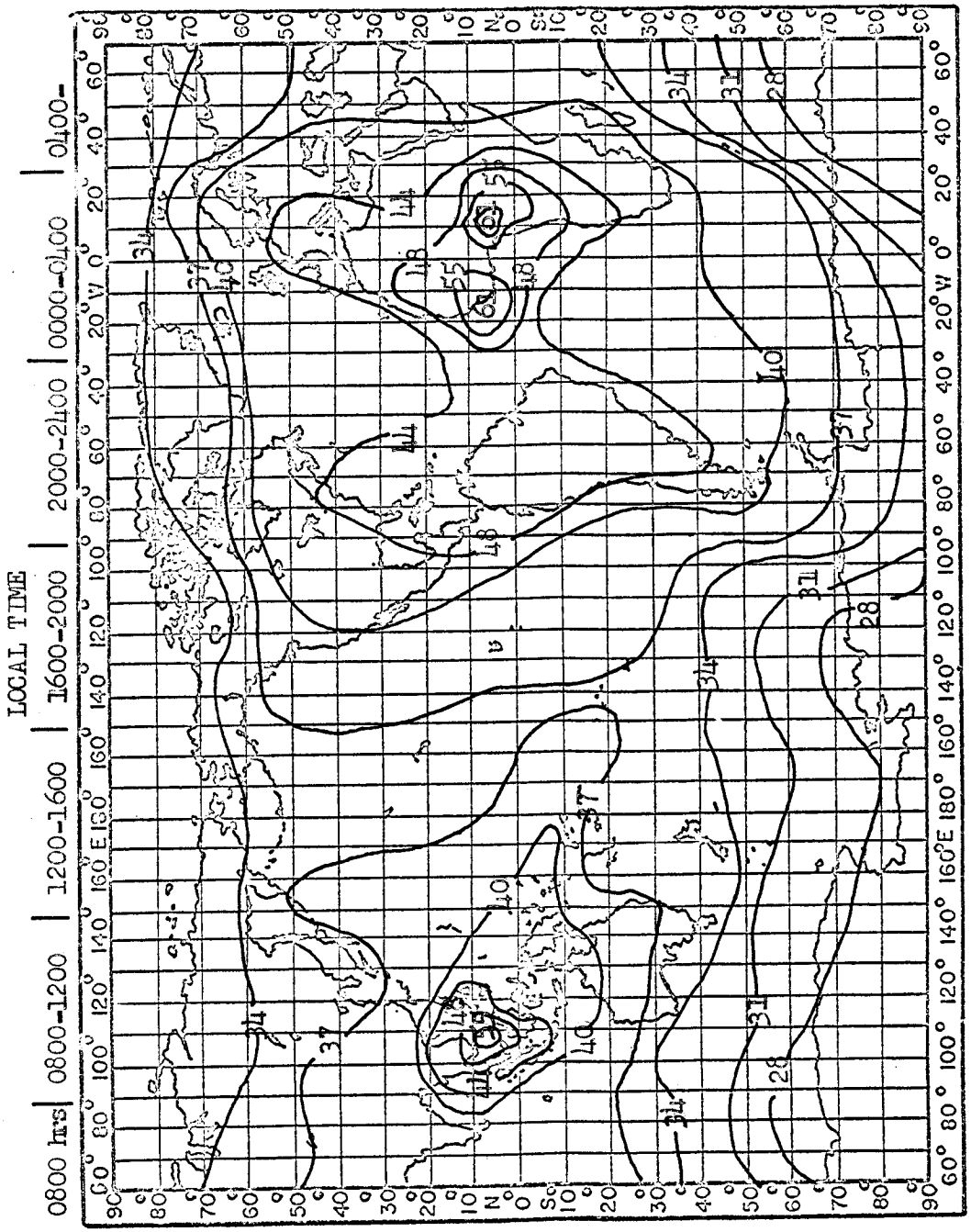

Figure 30. Expected values of radio noise (in db above 1 uv for 1 kc/s bandwidth) at 20 kc/s, from 0000-0400 hrs. Greenwich Time, for September, October, November.

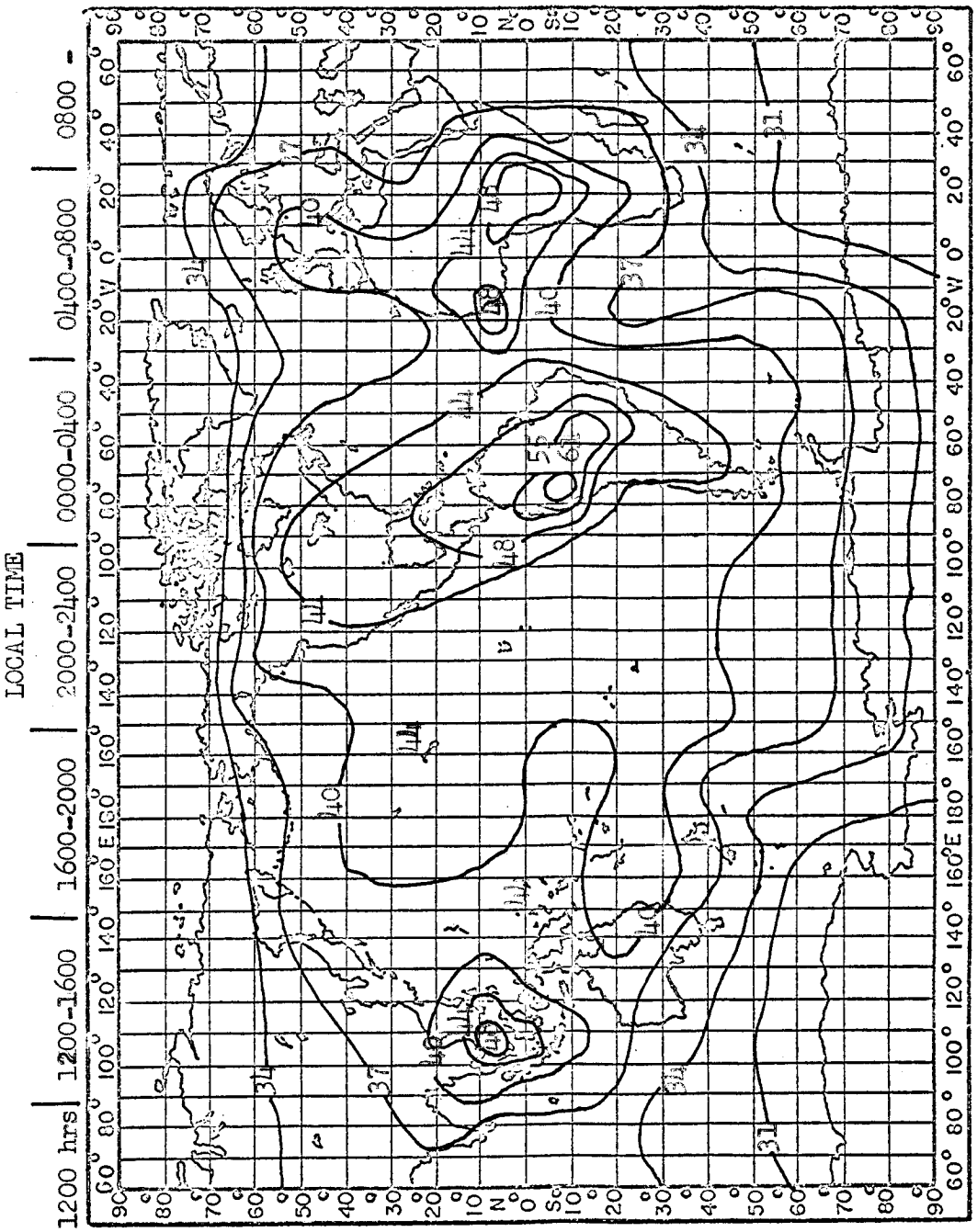

Figure 31. Expected values of radio noise (in db above 1 uv/m for 1 kc/s bandwidth) at 20 kc/s, from 0400-0800 hrs. Greenwich Time, for September, October, November.

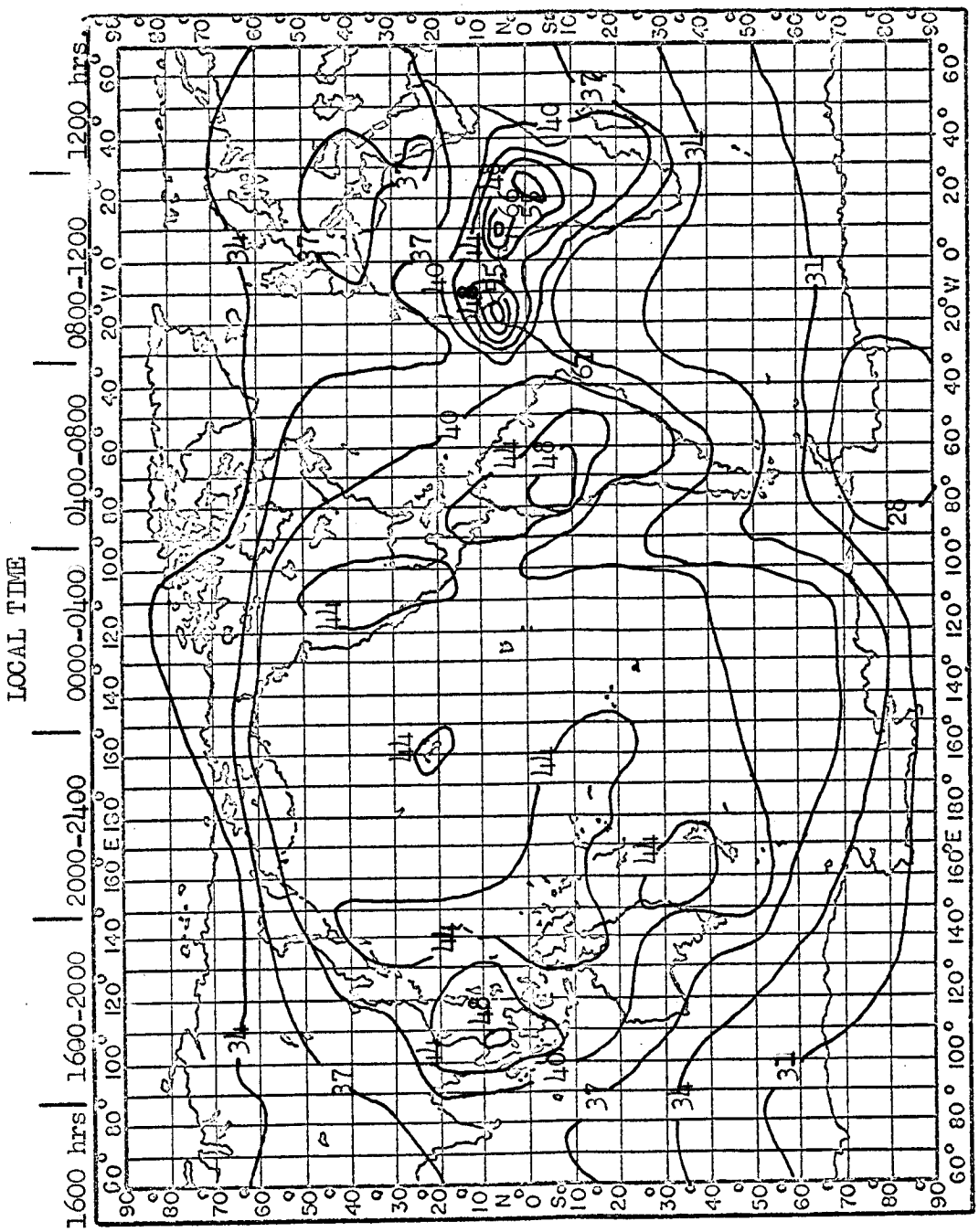

Figure 32. Expected values of radio noise (in db above 1 uv/m for 1 kc/s bandwidth) at 20 kc/s, from 0800-1200 hrs. Greenwich Time, for September, October, November.

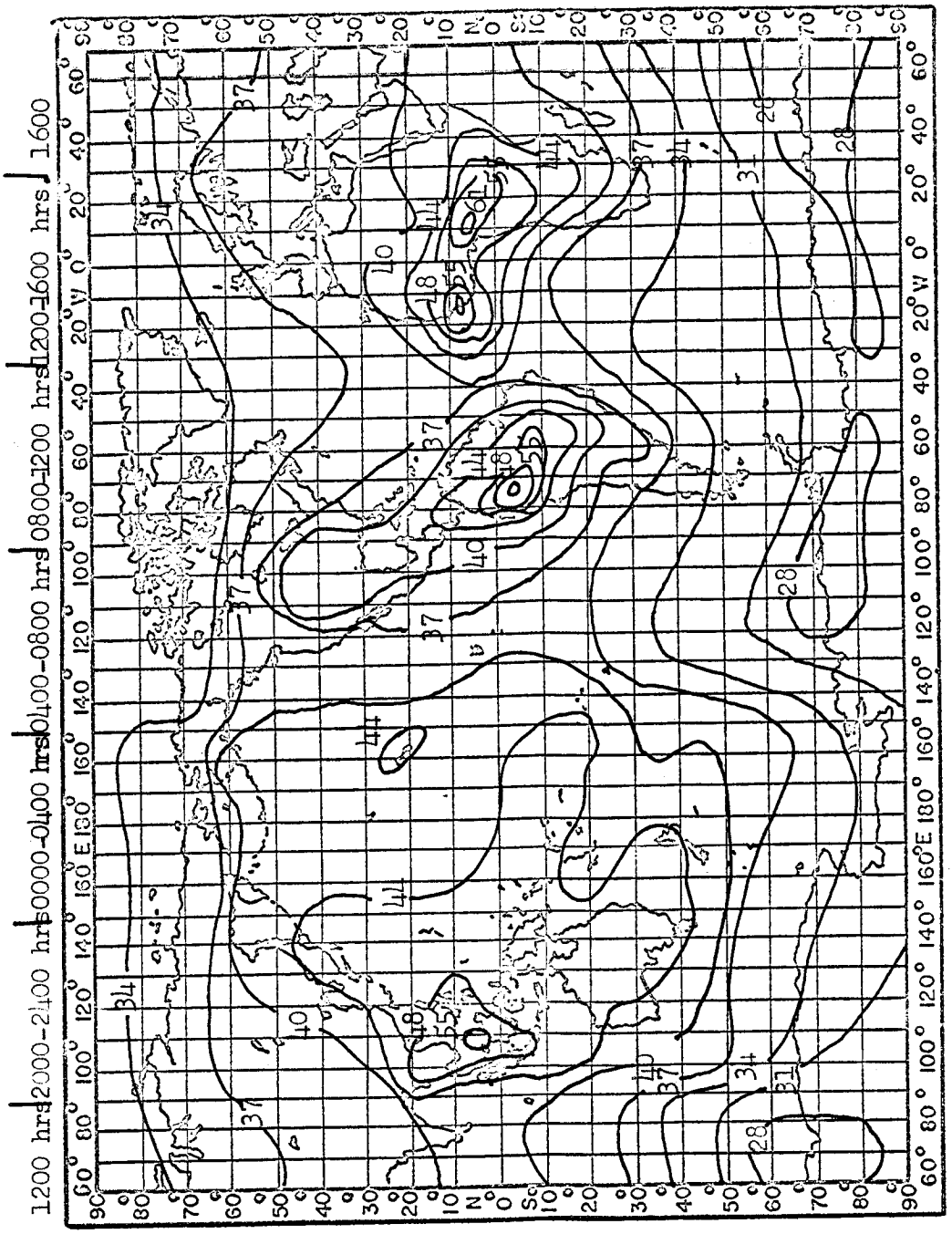

Figure 33. Expected Values of radio noise (in db above 1 uv/m for 1 kc/s bandwidth) at 21 kc/s, for 1200-1600 hrs. Greenwich Time, for September, October, November.

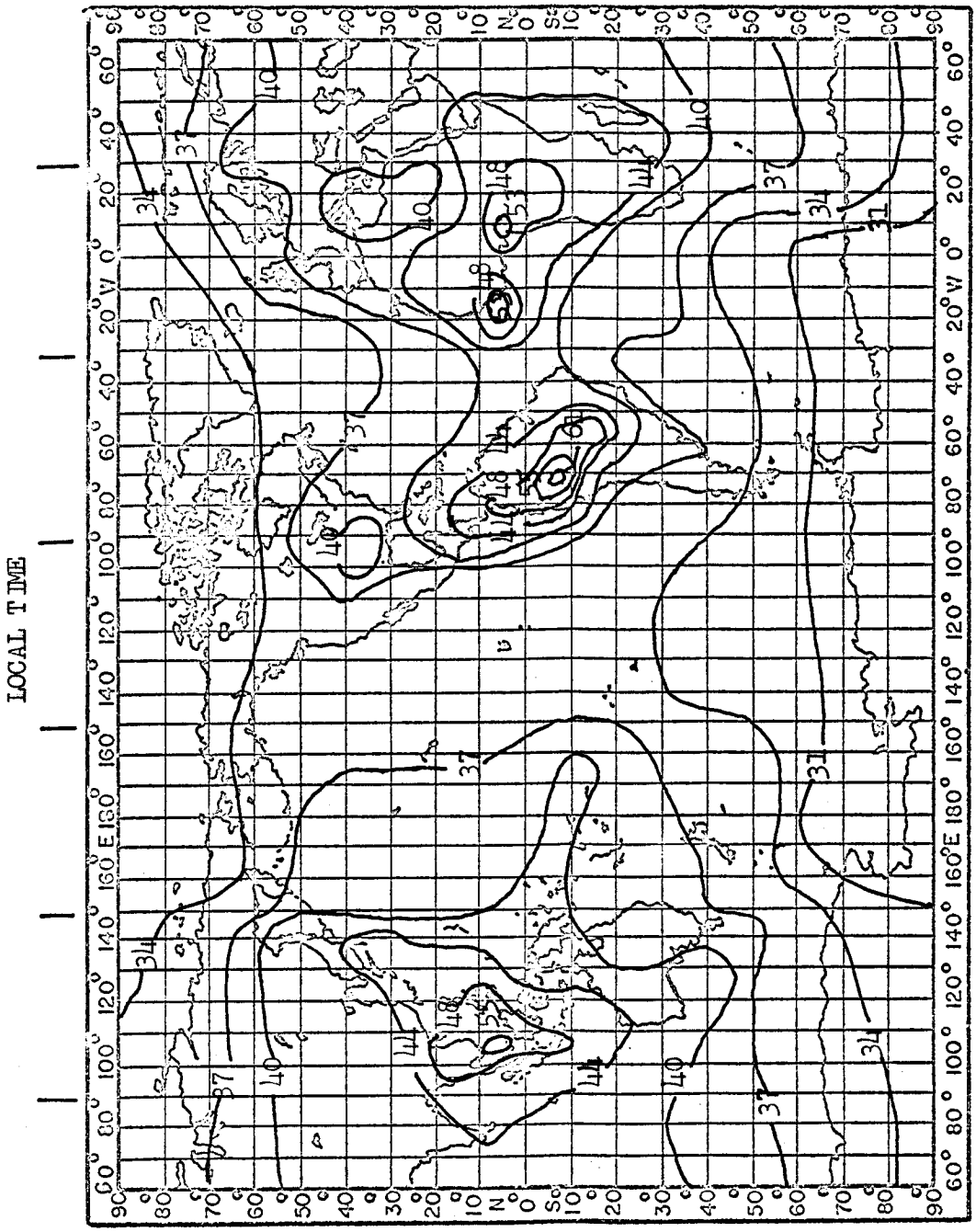

Figure 34. Expected values of radio noise (in db above 1 uv/m for 1 kc/s bandwidth) at 20 kc/s, from 1600-2000 hrs. Greenwich Time, for September, October, November.

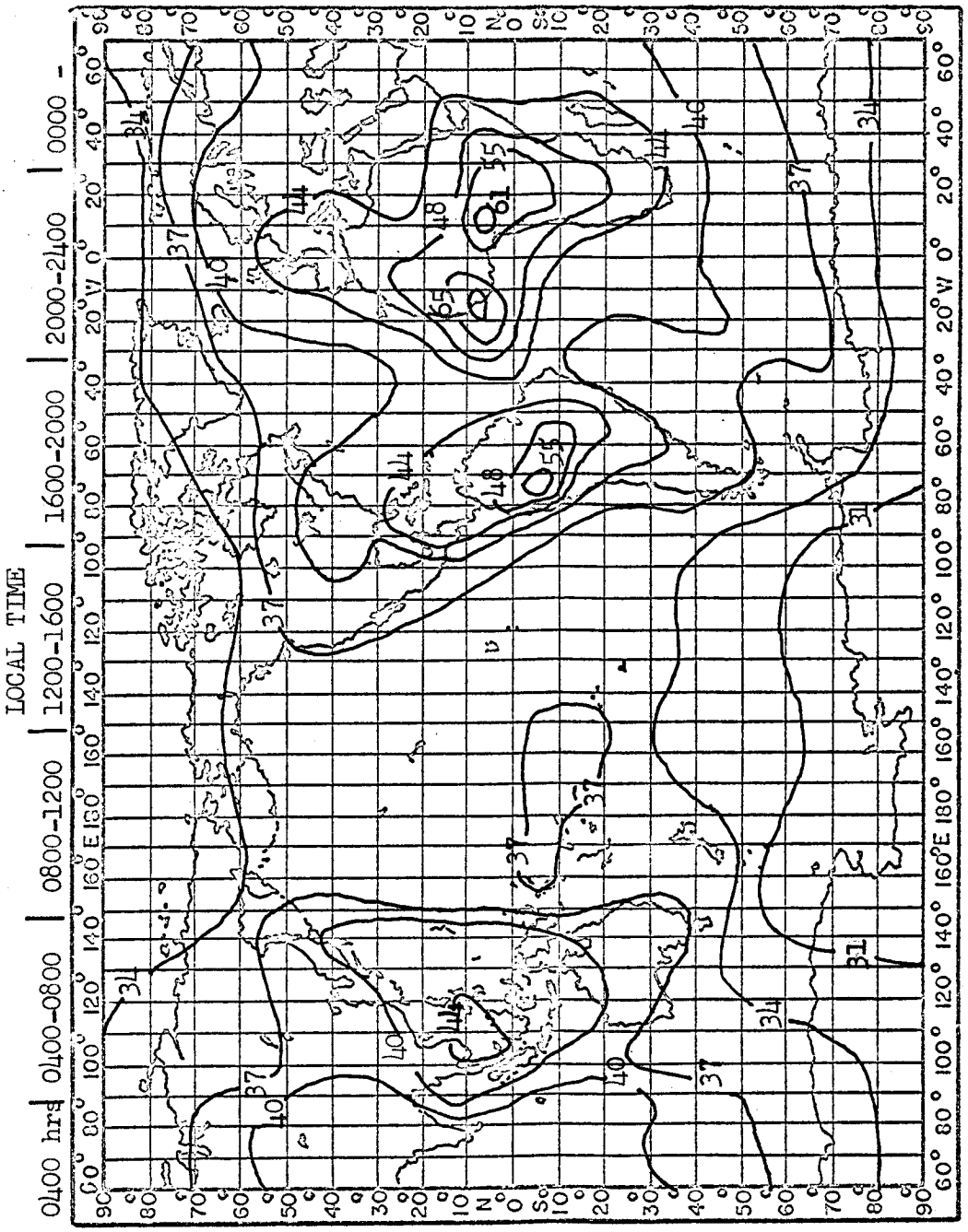

Figure 35. Expected values of radio noise (in db above 1 uv/m for 1 kc/s bandwidth) at 20 kc/s, from 2000-2400 hrs. Greenwich Time, for September, October, November.

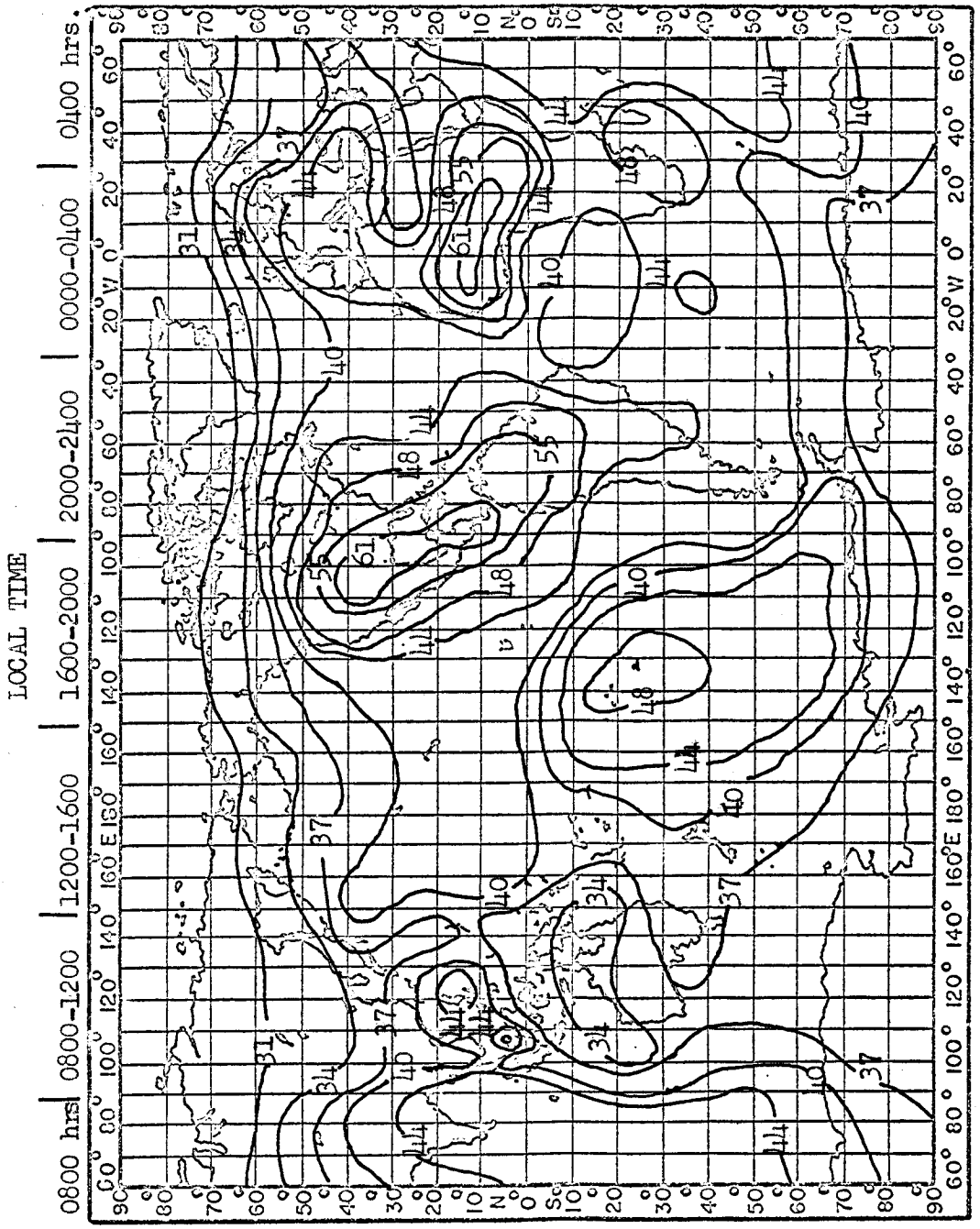

Figure 36. Expected values of radio noise (in db above 1 uw/m for 1 kc/s bandwidth) at 20 kc/s, from 0000-0400 hrs. Greenwich Time, for June, July, August.

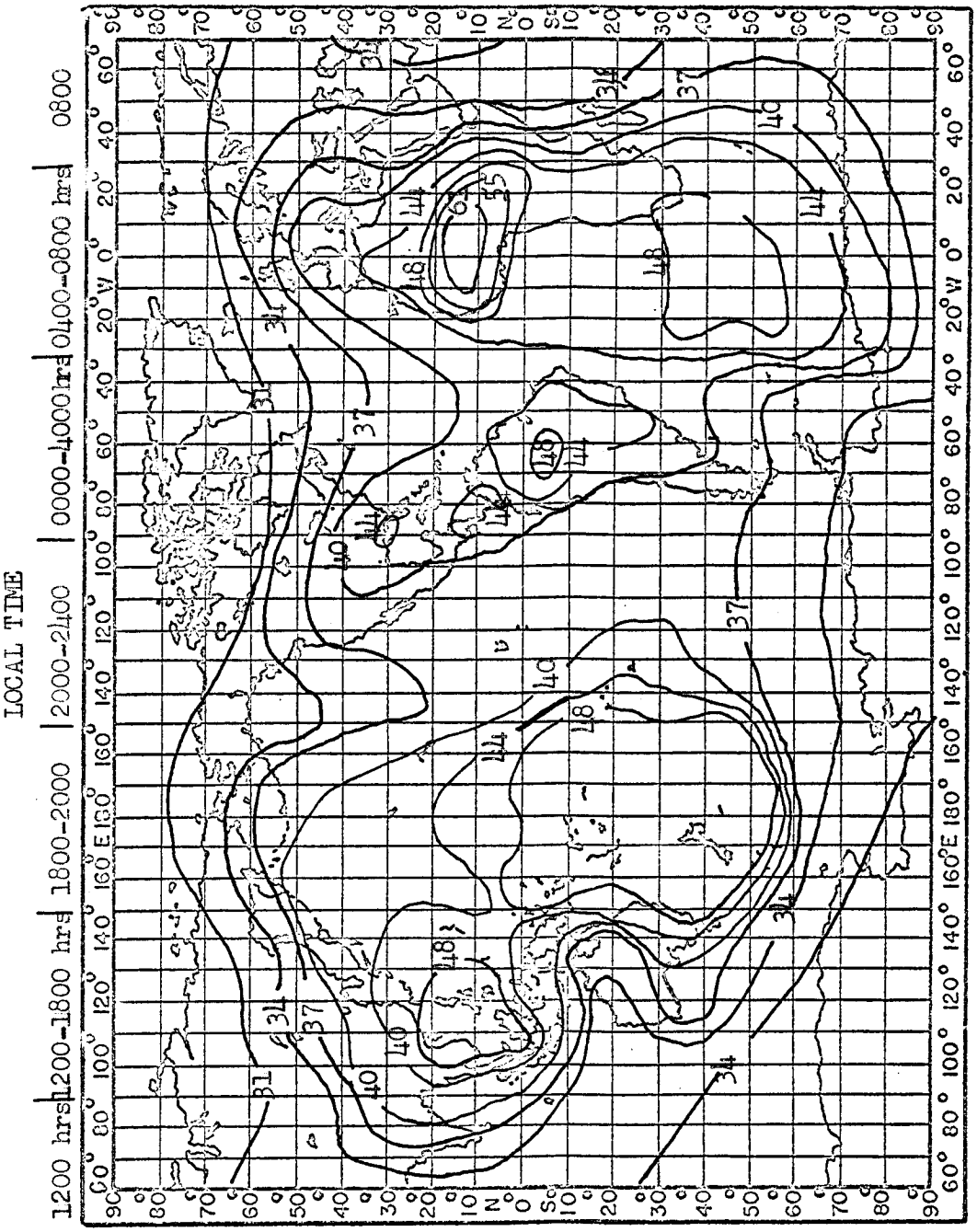

Figure 37. Expected values of radio noise (in db above 1 uv/m for 1 kc/s bandwidth) at 20 kc/s, from 0400-0800 hrs. Greenwich Time, for June, July, August.

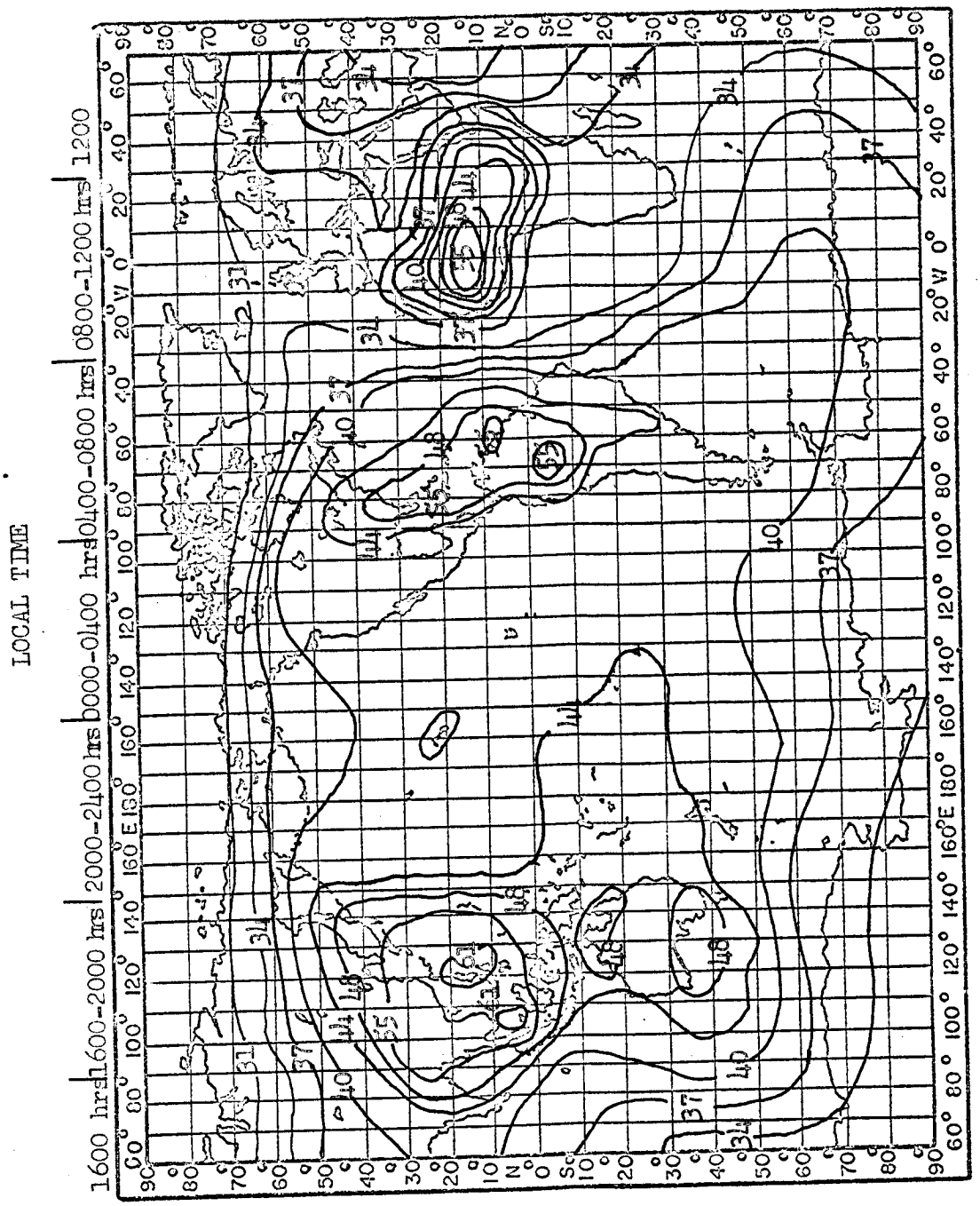

Figure 38. Expected values of radio noise (in db above 1 uv/m for 1 kc/s bandwidth) at 20 kc/s, from 0800-1200 hrs. Greenwich Time, for June, July, August.

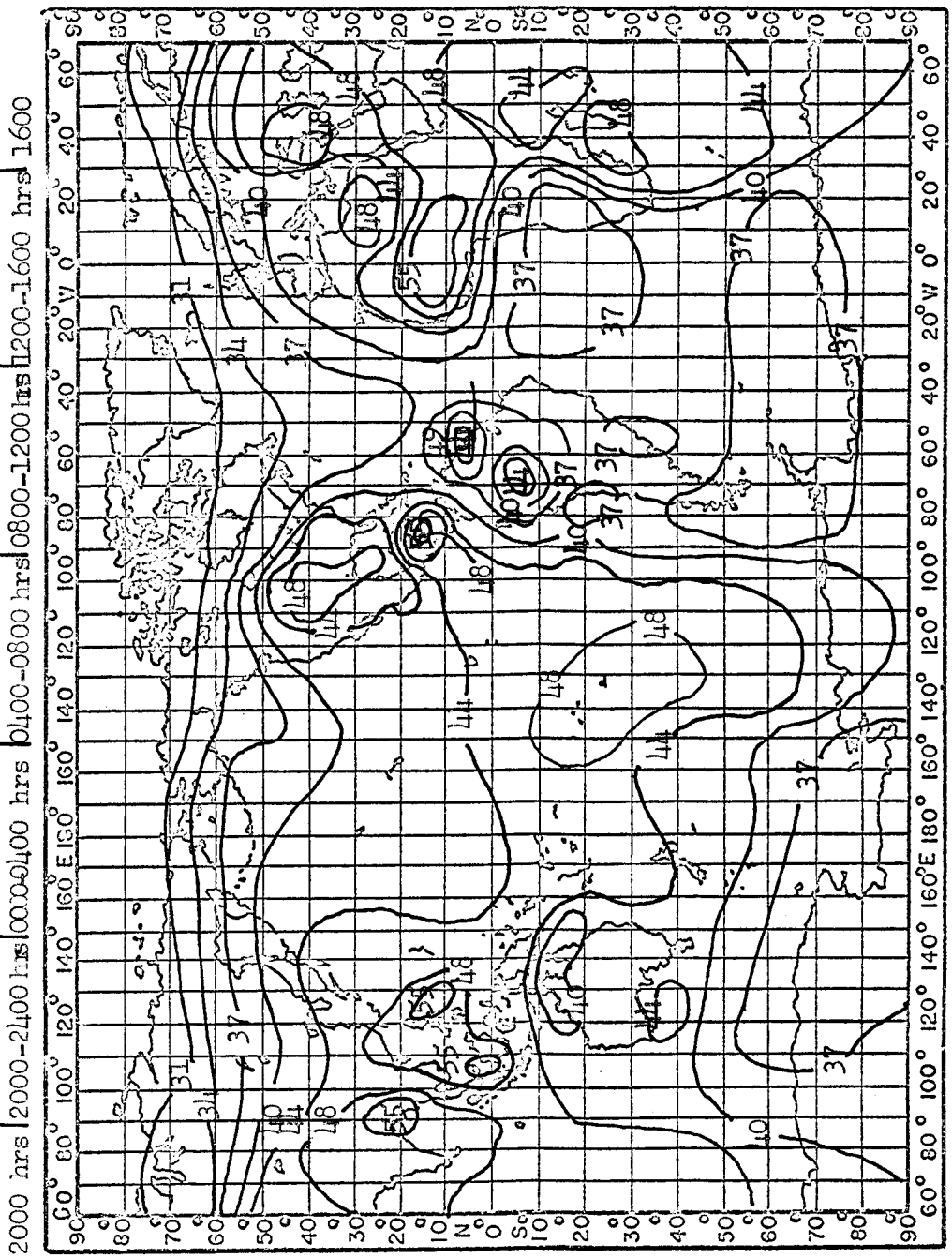

Figure 39. Expected values of radio noise (in db above 1 uv/m for 1 kc/s bandwidth) at 20 kc/s, from 1200-1600 hrs. Greenwich Time, for June, July, August.

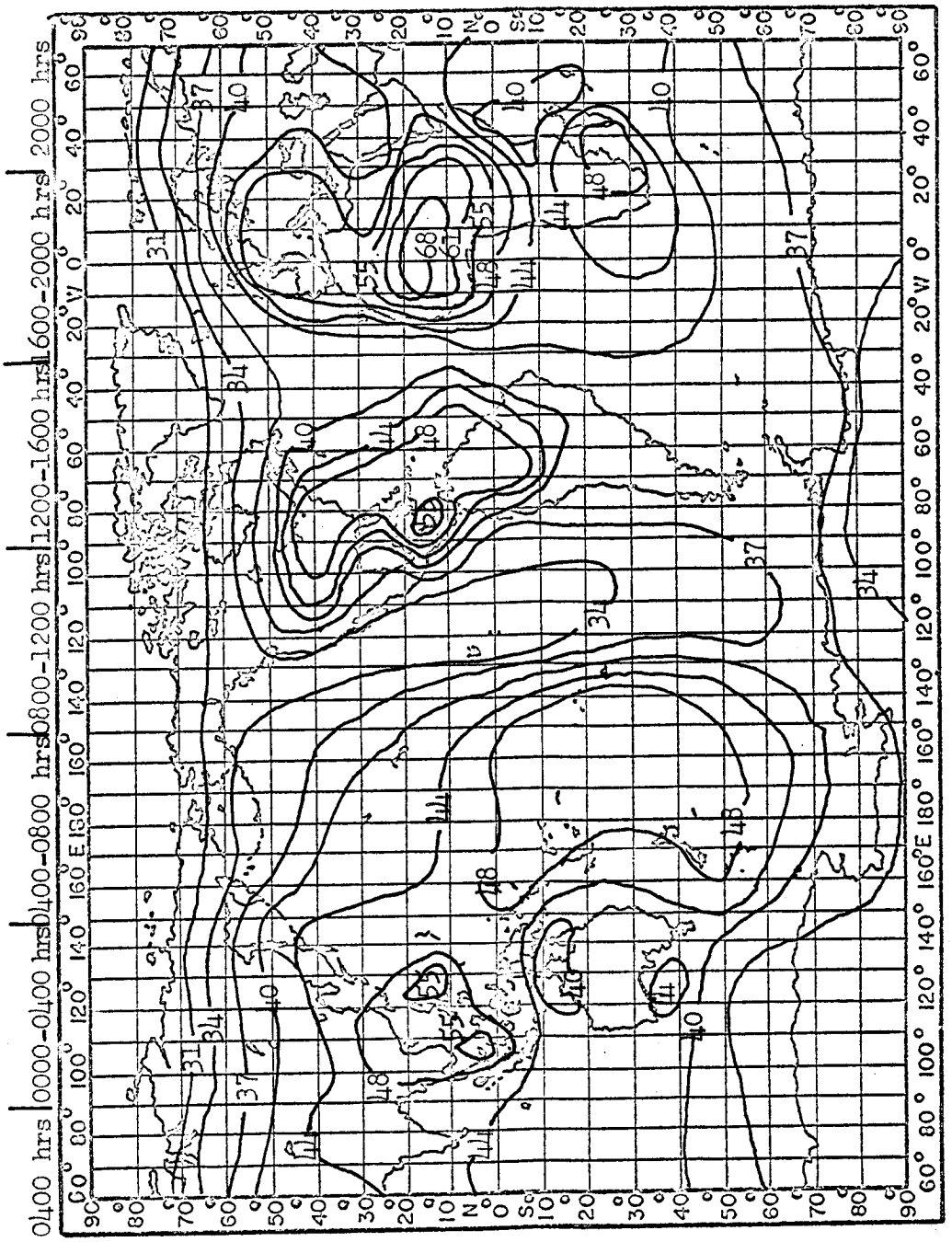

Figure 40. Expected values of radio noise (in db above 1 uv/m for 1 kc/s bandwidth) at 20 kc/s, from 1600-2000 hrs. Greenwich Time, for June, July, August.

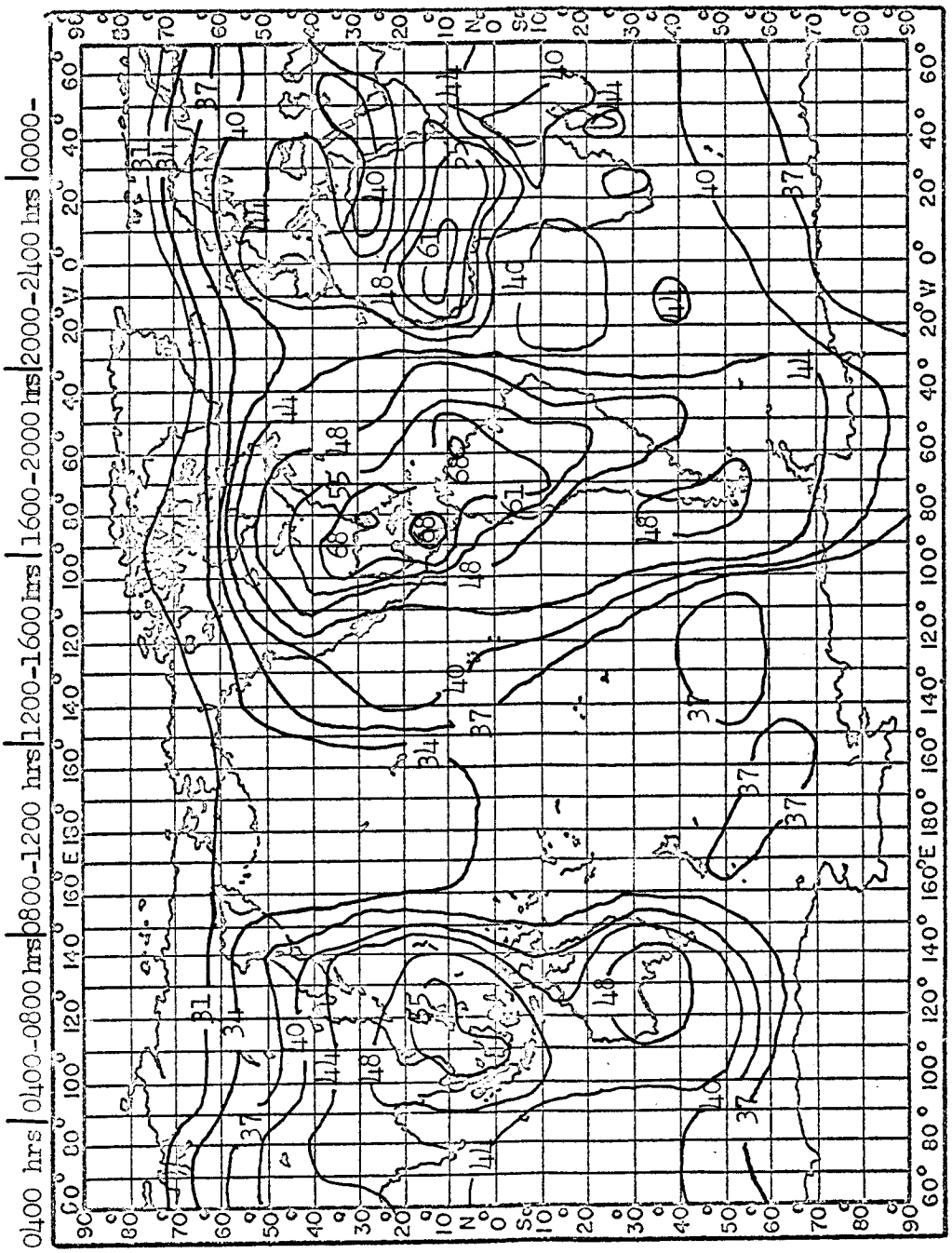

Figure 41. Expected values of radio noise (in db above 1 uv/m for 1 kc/s bandwidth) at 20 kc/s, from 2000-2400 hrs. Greenwich Time, for June, July, August.

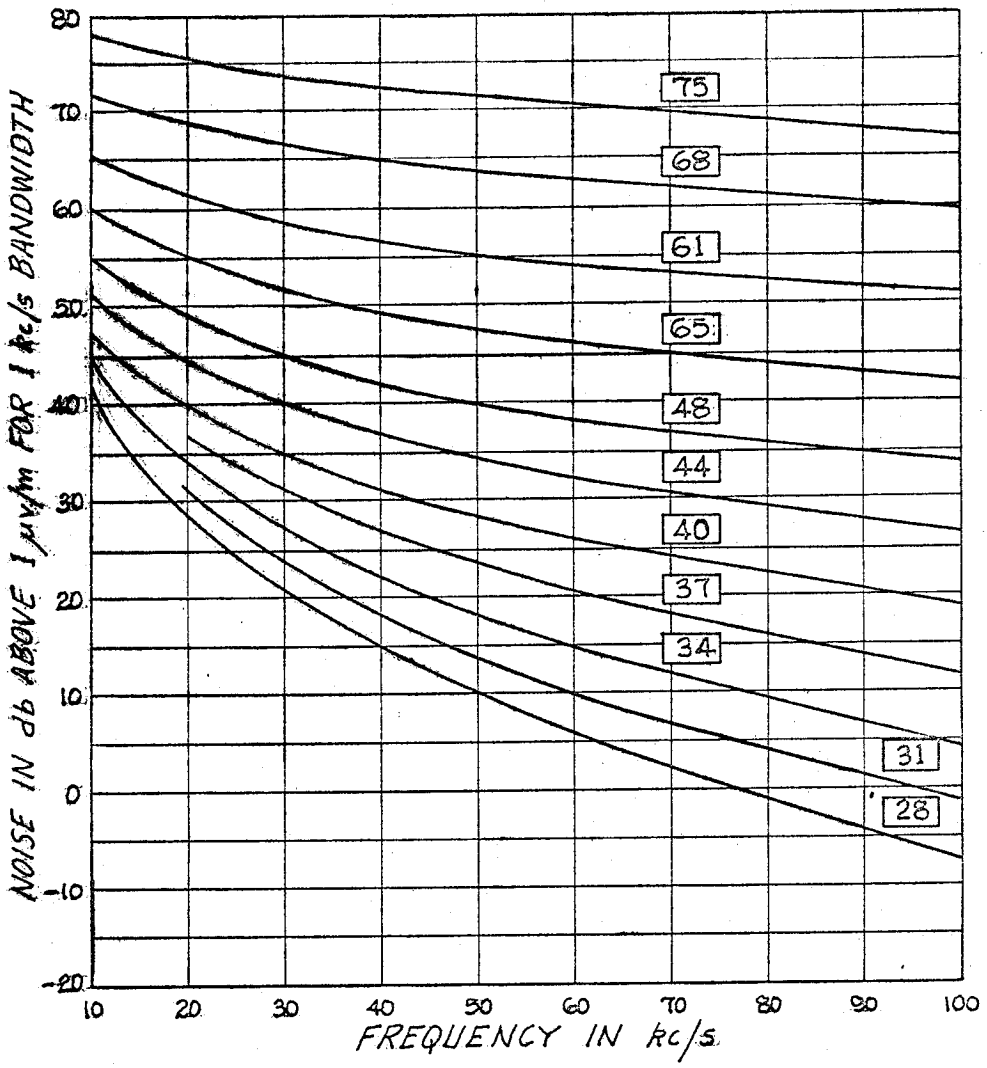

The figures in rectangles indicate the noise grades at 20 kc/s.

Figure 42.

Median values of radio noise expected for a short vertical antenna.